nature methods

ARTICLES

https://doi.org/10.1038/s41592-020-0953-2

An optimized acetylcholine sensor for monitoring in vivo cholinergic activity

Miao Jing[1]✉, Yuexuan Li[2,3,4], Jianzhi Zeng[2,3,5], Pengcheng Huang[6], Miguel Skirzewski[7], Ornela Kljakic[8,9,10], Wanling Peng[11], Tongrui Qian[2,3,5], Ke Tan[2,3], Jing Zou[12], Simon Trinh[12], Runlong Wu[13], Shichen Zhang[2,3], Sunlei Pan[2,3,5], Samuel A. Hires[12], Min Xu[11], Haohong Li[6], Lisa M. Saksida[8], Vania F. Prado[8,9,10], Timothy J. Bussey[8], Marco A. M. Prado[8,9,10], Liangyi Chen[2,13], Heping Cheng[2,13,14] and Yulong Li[2,3,5]✉

The ability to directly measure acetylcholine (ACh) release is an essential step toward understanding its physiological function. Here we optimized the GRAB$_{ACh}$ (GPCR-activation-based ACh) sensor to achieve substantially improved sensitivity in ACh detection, as well as reduced downstream coupling to intracellular pathways. The improved version of the ACh sensor retains the subsecond response kinetics, physiologically relevant affinity and precise molecular specificity for ACh of its predecessor. Using this sensor, we revealed compartmental ACh signals in the olfactory center of transgenic flies in response to external stimuli including odor and body shock. Using fiber photometry recording and two-photon imaging, our ACh sensor also enabled sensitive detection of single-trial ACh dynamics in multiple brain regions in mice performing a variety of behaviors.

Cholinergic signals mediated by the neurotransmitter ACh are involved in a wide range of physiological processes, including muscle contraction, cardiovascular function, neural plasticity, attention and memory[1–3]. Previously, cholinergic activity in vivo was mainly measured by electrophysiology recording of nicotinic receptor-mediated currents[4,5], by microdialysis followed with biochemical purification and identification[6], or, recently, by cell-based sensors such as CNiFERs that convert extracellular ACh dynamics to intracellular Ca^{2+} signaling for detection[7]. However, these methods generally lack both cell type specificity and the spatiotemporal resolution needed to precisely dissect cholinergic signals in the complex nervous system. Combining the type 3 muscarinic ACh receptor (M_3R) with circularly permutated GFP (cpGFP), we recently developed GACh2.0 (shortened to ACh2.0), a genetically encoded GRAB (GPCR-Activation-Based) ACh sensor that converts the ACh-induced conformational change on M_3R into a sensitive fluorescence response[8]. The ACh2.0 sensor responds selectively to physiological concentrations of ACh with a half-maximal effective concentration (EC_{50}) of 2 μM and has been used in several model organisms to detect the endogenous release and regulation of cholinergic signals[9,10]. Here we optimized the GRAB$_{ACh}$ sensor using site-directed mutagenesis and cell-based screening to further improve its performance in ACh detection.

Results

Engineering and characterization of ACh3.0 in cultured cells. To improve the sensitivity of the GRAB$_{ACh}$ sensor, we focused on the interface between M_3R and cpGFP, including the receptor's third intracellular loop (ICL3) and linker peptides, as well as critical residues in cpGFP that contribute to its fluorescence intensity (Fig. 1a and Extended Data Figs. 1 and 2). Our initial screening based on medium-throughput imaging on HEK293T cells identified several variants with improved performance; we subsequently verified these variants using confocal microscopy (see Methods for details). We selected the sensor with the largest ACh-induced fluorescence response for further study and named it GRAB$_{ACh3.0}$, or ACh3.0 (Fig. 1a). We also generated a ligand-insensitive form of ACh3.0 (ACh3.0-mut) by introducing a W200A substitution into the receptor[11] (Fig. 1a and Extended Data Fig. 1e). When expressed in HEK293T cells or cultured neurons, the ACh3.0 sensor localized to the plasma membrane of the soma and trafficked to dendrites and axons in neurons (Fig. 1b–d). Moreover, when compared to ACh2.0, the ACh3.0 sensor had a significantly larger change in fluorescence in response to 100 μM ACh ($\Delta F/F_0$ of ~280% and ~76% for ACh3.0 and ACh2.0 in HEK293T cells, respectively; $P = 6.26 \times 10^{-6}$, two-sided Student's t test) (Fig. 1b–d and Extended Data Fig. 3a–e); in contrast, the ACh-induced change in fluorescence for the

[1]Chinese Institute for Brain Research, Beijing, China. [2]State Key Laboratory of Membrane Biology, Peking University School of Life Sciences, Beijing, China. [3]PKU-IDG/McGovern Institute for Brain Research, Beijing, China. [4]Peking University Health Science Center, Beijing, China. [5]Peking-Tsinghua Center for Life Sciences, Academy for Advanced Interdisciplinary Studies, Peking University, Beijing, China. [6]Britton Chance Center for Biomedical Photonics, Wuhan National Laboratory for Optoelectronics; MoE Key Laboratory for Biomedical Photonics, Collaborative Innovation Center for Biomedical Engineering, School of Engineering Sciences, Huazhong University of Science and Technology, Wuhan, China. [7]BrainsCAN Rodent Cognition Core, The University of Western Ontario, London, Ontario, Canada. [8]Robarts Research Institute, Department of Physiology and Pharmacology, Schulich School of Medecine and Dentistry, Brain and Mind Institute, The University of Western Ontario, London, Ontario, Canada. [9]Department of Anatomy and Cell Biology, The University of Western Ontario, London, Ontario, Canada. [10]Department of Anatomy and Cell Biology, Brain and Mind Institute, The University of Western Ontario, London, Ontario, Canada. [11]Institute of Neuroscience, State Key Laboratory of Neuroscience, CAS Center for Excellence in Brain Science and Intelligence Technology, Chinese Academy of Sciences, Shanghai, China. [12]Department of Biological Sciences, Section of Neurobiology, University of Southern California, Los Angeles, CA, USA. [13]Institute of Molecular Medicine, Peking University, Beijing, China. [14]Research Unit of Mitochondria in Brain Diseases, Chinese Academy of Medical Sciences, PKU-Nanjing Institute of Translational Medicine, Nanjing, China. ✉e-mail: jingmiao@cibr.ac.cn; yulongli@pku.edu.cn

ACh3.0-mut sensor ($\Delta F/F_0$ of ~1.8%) was less than 0.6% as large as the change for ACh3.0, even at the highest ACh concentration tested (100 μM) (Fig. 1b–d and Extended Data Fig. 1f). To probe the response kinetics of ACh3.0, we locally puffed cells with different concentrations of ACh and obtained a rate constant for ACh of $k_{on} = 3.12\,s^{-1}\,\mu M^{-1}$ for ACh3.0 on the basis of the kinetics of the change in fluorescence and ACh concentration (Fig. 1e–g and Extended Data Fig. 3f). We similarly calculated the disassociation rate constant ($k_{off} = 1.72\,s^{-1}$) of ACh3.0 for ACh by puffing cells with antagonist (tiotropium, Tio[12]; 10 μM) while they were bathed in ACh (100 μM) (Fig. 1e–g and Extended Data Fig. 3g). The kinetic properties of ACh3.0 are similar to those of endogenous muscarinic ACh receptors[13,14]. Importantly, ACh3.0 had a similar EC_{50} (~2 μM) as ACh2.0 when we characterized the dose-dependent response to different concentrations of ACh and did not respond to nicotine and other major neurotransmitters (Fig. 1h,i). Using multiple assays, including intracellular Ca^{2+} imaging, the G_q-dependent luciferase complementation assay[15] and the β-arrestin-dependent TANGO assay[16], we confirmed that ACh3.0 had negligible coupling with major G-protein-coupled receptor (GPCR)-mediated downstream pathways (Fig. 1j,k and Extended Data Fig. 4a–e). We also showed that expressing ACh3.0 does not affect the physiological properties of neurons, as odorant-evoked Ca^{2+} transients in *Drosophila melanogaster* expressing both ACh3.0 and jRCaMP1a[17] were similar to those in flies expressing only jRCaMP1a (Extended Data Fig. 4f,g).

Detecting cholinergic activity in acute brain slices and in vivo in *Drosophila* with ACh3.0. We previously reported that the ACh2.0 sensor could be used to record endogenous ACh dynamics, including the γ-aminobutyric acid $(GABA)_B$ receptor ($GABA_BR$)-dependent potentiation of ACh release in the medial habenula (MHb)–interpeduncular nucleus (IPN) projection in acute mouse brain slices[8,18]. We next tested whether ACh3.0 had better performance than ACh2.0 in reporting ACh release evoked by electrical stimulation in MHb–IPN slices (Fig. 2a). In line with our in vitro results, the ACh3.0 sensor had a significantly larger fluorescence increase than ACh2.0 in response to high-frequency (>10-Hz) electrical stimulation of the cholinergic fibers, both in control artificial cerebrospinal fluid (ACSF) solution and in the presence of the $GABA_BR$ agonist baclofen ($P = 7.21 \times 10^{-11}$ in ACSF and $P = 6.69 \times 10^{-6}$ in baclofen, all at 100 Hz, two-sided Student's *t* test) (Fig. 2b,c and Extended Data Fig. 5a–f). Application of the $GABA_BR$ antagonist saclofen reversed the baclofen-induced potentiation, and further adding Tio eliminated the stimulation-evoked response (Fig. 2d). Moreover, the electrically evoked signal was increased by the K^+ channel blocker 4-AP and eliminated by Cd^{2+}, in line with Ca^{2+}-dependent ACh release (Fig. 2e and Extended Data Fig. 5g–i). Using a 100-ms electrical stimulation, we then measured the kinetics of the fluorescence response, yielding τ_{on} and τ_{off} values of approximately 105 ms and 3.7 s, respectively (Fig. 2f).

Next, we used in vivo two-photon imaging to compare the performance of ACh3.0 and ACh2.0 in transgenic *Drosophila* expressing the ACh sensors in Kenyon cells (KCs) of the olfactory mushroom body[19] (Fig. 2g). Physiologically relevant stimuli, including body shock to the abdomen and odor stimulation, elicited only a minor fluorescence signal in the horizontal lobe of the mushroom body in ACh2.0-expressing flies. In contrast, the same stimuli induced a significantly larger response in ACh3.0-expressing flies ($P = 0.038$ for body shock and $P = 1.26 \times 10^{-7}$ for odor, two-sided Student's *t* test), and this increase was higher in the γ3 lobe than in the adjacent γ2 lobe, revealing compartment-specific release of ACh (Fig. 2g,h). In addition, we monitored ACh dynamics in response to direct neuronal activation of KCs via CsChrimson-mediated optogenetics[20] or electrical stimulation. A single pulse from a 635-nm laser evoked a

Fig. 1 | Optimization and in vitro characterization of next-generation $GRAB_{ACh}$ sensors. a, Left, cartoon illustration showing the predicted structure of $GRAB_{ACh}$ sensors. Right, site-directed random mutagenesis was performed in linkers between the receptor and cpEGFP (magenta), cpEGFP (green) or both (orange), and the performance of each variant (relative to ACh2.0, black) was calculated. The final optimized sensor, ACh3.0, is indicated in red, and the ligand-insensitive ACh3.0-mut sensor (with a W200A substitution) is indicated in gray. Each data point represents the average response measured in >100 cells per candidate. The 'relative response' was calculated by considering $\Delta F/F_0$ for ACh2.0 as 1 and normalizing $\Delta F/F_0$ for each candidate to this. The 'relative brightness' was calculated similarly. The crystal structures are from the Protein Data Bank (PDB) archive (4DAJ for M_3R and 3EK4 for cpGFP). **b**, The performance of the ACh2.0, ACh3.0 and ACh3.0-mut sensors expressed in HEK293T cells in response to 100 μM ACh upon confocal imaging. Top, pseudocolored images of the peak response ($\Delta F/F_0$) in the presence of 100 μM ACh. Bottom, representative traces and group data; $n = 5$, 7 and 4 coverslips for ACh2.0, ACh3.0 and ACh3.0-mut, respectively, with an average of >20 cells per coverslip; $P = 6.2 \times 10^{-6}$ for the comparison of ACh2.0 and ACh3.0, $P = 9.9 \times 10^{-6}$ for the comparison of ACh3.0 and ACh3.0-mut. **c**, The performance of the ACh2.0, ACh3.0 and ACh3.0-mut sensors expressed in cultured rat cortical neurons in response to 100 μM ACh. The raw GFP fluorescence and pseudocolored images of the peak response to ACh ($\Delta F/F_0$) and signal-to-noise ratio (SNR) are shown. Similar results as the representative images were observed for more than ten neurons. **d**, Left, representative images of ACh3.0 expressed together with synaptophysin (Syp) or CAAX fused to mScarlet. Dendritic spines are indicated by white arrowheads. Right, group data summarizing the fluorescence response of ACh2.0 (black bars) and ACh3.0 (red bars) to 100 μM ACh measured in the indicated neuronal compartments (cell body: $n = 11$ cells for ACh2.0 and $n = 18$ cells for ACh3.0, $P = 5.1 \times 10^{-14}$; axon: $n = 8$ cells for ACh2.0 and $n = 14$ cells for ACh3.0, $P = 2.3 \times 10^{-13}$; dendrite: $n = 18$ cells for ACh2.0 and $n = 26$ cells for ACh3.0, $P = 4.6 \times 10^{-15}$; spine: $n = 10$ cells for ACh2.0 and $n = 16$ cells for ACh3.0, $P = 1.5 \times 10^{-13}$). **e**, The raising kinetics of ACh3.0 fluorescence signal in HEK293T cells in response to locally puffed ACh at the indicated concentrations in the puffing pipette. The actual concentrations reaching the cell were calibrated in Extended Data Fig. 3g on the basis of the peak fluorescence response of ACh3.0. Representative traces and group data are shown ($n = 6$ cells for 1 μM ACh, $n = 6$ cells for 10 μM ACh, $n = 8$ cells for 100 μM ACh and $n = 6$ cells for 1,000 μM ACh). **f**, The association rate constant of the ACh3.0 sensor for ACh. Local ACh concentrations were estimated on the basis of the dose-dependent fluorescence response of ACh3.0 ($n = 6$ cells for 1 μM ACh, $n = 6$ cells for 10 μM ACh, $n = 8$ cells for 100 μM ACh and $n = 6$ cells for 1,000 μM ACh; ACh concentrations here indicate those in the puffing pipette). **g**, The decay kinetics of the ACh3.0 fluorescence signal when cells were locally puffed with the antagonist Tio (10 μM) while bathed in ACh (100 μM). Representative traces and group data are shown ($n = 6$ cells from 6 coverslips). **h**, Dose–response relationship for the fluorescence responses of ACh2.0 (black), ACh3.0 (red) and ACh3.0-mut (gray) to ACh, with corresponding EC_{50} values ($n = 11$, 12 and 16 neurons for ACh2.0, ACh3.0 and ACh3.0-mut, respectively). **i**, The fluorescence response of ACh3.0 to the indicated compounds ($n = 12$ neurons each). ACh, 100 μM; nicotine (Nic), 50 μM; 5-hydroxytryptamine (5-HT), 1 μM; norepinephrine (NE), 10 μM; dopamine (DA), 20 μM; glutamate (Glu), 10 μM; Tio, 2 μM; $P = 3.5 \times 10^{-14}$, 2.0×10^{-14}, 2.3×10^{-14}, 7.2×10^{-14}, 6.9×10^{-14} and 7.5×10^{-14} for comparisons between ACh and Nic, 5-HT, NE, DA, Glu and ACh + Tio, respectively. **j**, The normalized Ca^{2+} response to ACh in HEK293T cells expressing GFP–M_3R or ACh3.0. Each data point is the average from $n = 10$ cells. **k**, The β-arrestin-dependent luminescence signal in HEK293T cells expressing GFP–M_3R or ACh3.0 in response to ACh at the indicated concentration ($n = 6$ wells in each group, with >100 cells per well). AU, arbitrary units. All data are shown as the mean ± s.e.m., with the error bars or shaded regions indicating s.e.m. Scale bars represent 10 μm, except in c, where the scale bar represents 20 μm. Two-sided Student's *t* tests were performed in **b**, **d** and **i**: ***$P < 0.001$; NS, not significant.

clear increase in ACh3.0 fluorescence, and multiple pulses applied at 10 Hz induced a progressive response increase that was largely eliminated by Tio application (Fig. 2i,j). Electrical stimulation of KCs confirmed the frequency-dependent fluorescence increase in the ACh3.0 sensor, with rapid kinetics (τ_{on} of ~0.09 s and τ_{off} of ~0.91 s) (Extended Data Fig. 6). Taken together, these data show

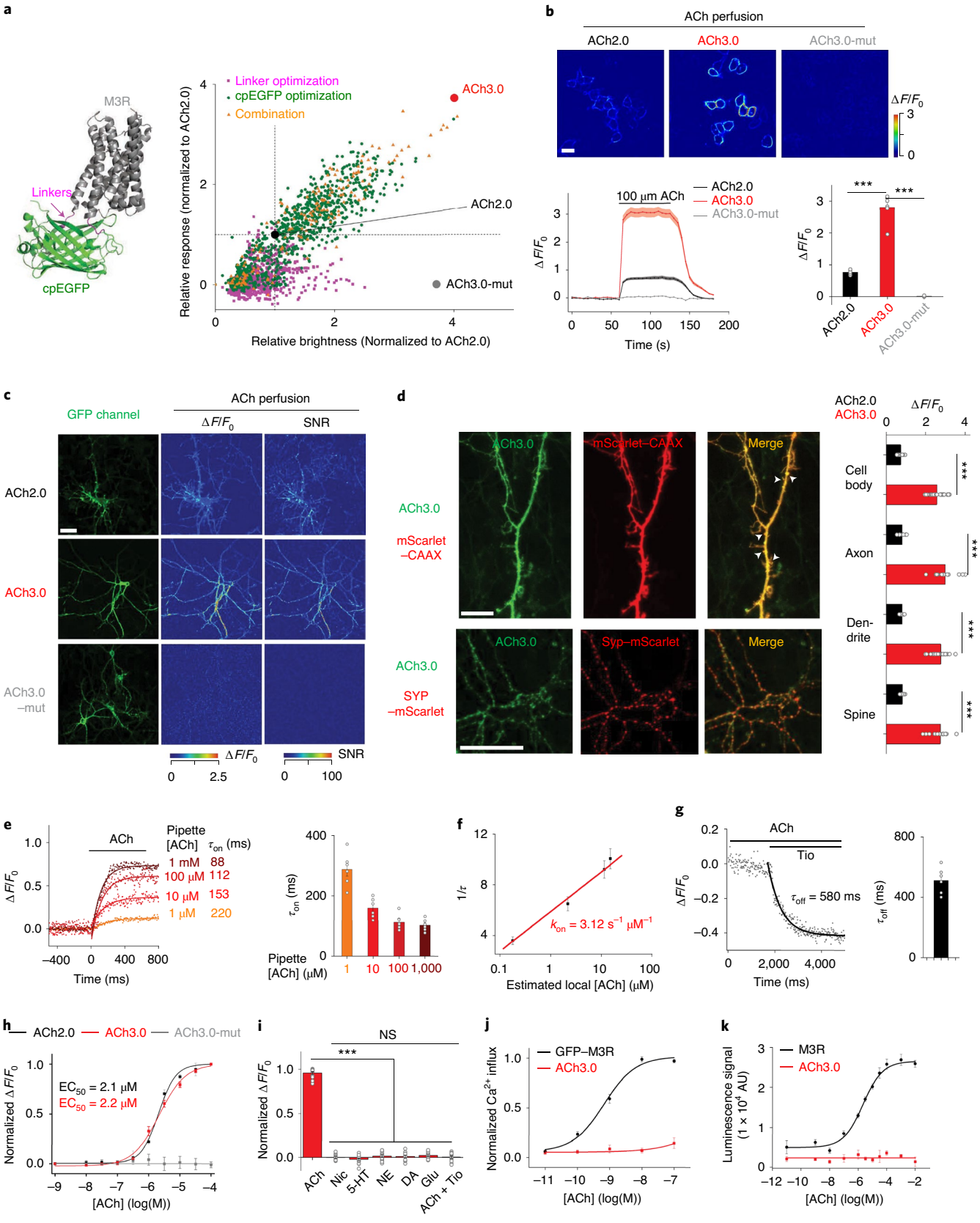

that the ACh3.0 sensor can reliably detect ACh release with high sensitivity and spatiotemporal resolution.

Recording of ACh dynamics in mice performing behaviors in vivo. Cholinergic signaling has a key role in modulating a variety of physiological processes, including plasticity and arousal[21–23]. We therefore examined whether ACh3.0 could be used in vivo to monitor ACh release in mice performing behaviors. In the mouse brain, basal forebrain cholinergic neurons project to the amygdala, hippocampus and cortical regions[24]. We measured foot-shock-evoked cholinergic signals in the basolateral amygdala (BLA), which is important for aversive associative learning[23]. A brief foot shock induced a reproducible and time-locked increase in ACh3.0 fluorescence (Fig. 3a,b). We then combined pharmacological and genetic manipulations to confirm the signal's specificity. Treating the mice with the acetylcholinesterase inhibitor (AChEI) donepezil[25] slowed the fluorescence decay, while the M_3R antagonist scopolamine abolished the foot-shock-induced fluorescence response (Fig. 3c). In control experiments, we did not observe a response in mice expressing ACh3.0-mut (Fig. 3d) or in mice lacking the vesicular ACh transporter ($VAChT^{-/-}$ mice, gene symbol *SLC18A3*)[26], suggesting a synaptic origin for the ACh release (Fig. 3e and Extended Data Fig. 7a–c). Foot shocks induced a much larger fluorescence response in the ACh3.0 sensor than in ACh2.0 ($\Delta F/F_0 = 88.4\%$ and 49.4% for ACh3.0 and ACh2.0, respectively; Extended Data Fig. 7d,e) in the BLA. Taken together, these in vivo data indicate that the ACh3.0 sensor can reliably and sensitively report foot-shock-induced cholinergic signaling in the BLA. Next, we examined whether ACh3.0 could stably report ACh signaling over a longer time period by recording ACh dynamics in the mouse hippocampus during the sleep–wake cycle. We simultaneously recorded an electroencephalogram (EEG) and an electromyogram (EMG) to monitor the animal's sleep status (Fig. 3f). We found that the average fluorescence signal was larger during wakefulness and REM sleep but lower during non-REM (NREM) sleep (Fig. 3g,h and Extended Data Fig. 8), in line with our previous optrode-based recordings of the firing rate of basal forebrain cholinergic neurons[27]. In control experiments, we observed significantly smaller fluorescence changes during sleep–wake cycles when using the ACh3.0-mut sensor as compared to ACh3.0 ($P = 0.0009$ during wakefulness, $P = 0.049$ in NREM, $P = 0.008$ in REM, two-sided Student's t test) (Fig. 3h and Extended Data Fig. 8). ACh3.0 was also able to detect ACh increases induced by microarousal events during NREM sleep (Fig. 3g), illustrating its precise temporal resolution in ACh detection. Overall, these data show that ACh3.0 has the high sensitivity, rapid kinetics and stability needed to reliably track long-term physiological cholinergic signals in vivo.

Next, to demonstrate the applicability of ACh3.0 in tracking cholinergic signaling with high spatiotemporal resolution during volitional behavior, we performed two-photon imaging of ACh3.0 in the primary somatosensory cortex (S1) of head-fixed mice performing a go/no-go whisker-guided object location discrimination task[28] (Fig. 3i; see Methods for details). Briefly, mice explored a presented pole with a whisker during the sampling period. During the answer period, mice licked for a water reward when the pole was proximal (hit trials) and withheld licking when the pole was distal (correct rejection trials). The presentation of a pole triggered a modest increase in ACh in both hit and correct rejection trials during the sampling period (Fig. 3j,k). Furthermore, correct licking during the answer period (hit trials) drove large increases in ACh, which were sustained at a more modest level until the end of the trial (Fig. 3j,k and Extended Data Fig. 9). Application of scopolamine (5 mg per kg, intraperitoneally) largely reduced the fluorescence response on both correct rejection ($\Delta F/F_0 = 0.56\%$ before scopolamine and 0.01% after scopolamine) and hit ($\Delta F/F_0 = 4.35\%$ before scopolamine and 1.91% after scopolamine) trials (Fig. 3j,k). Scopolamine did not completely block the response on hit trials, likely owing to the non-saturating concentration of scopolamine applied because mice treated with a higher concentration fail to perform this behavioral task. Under the same experimental settings, ACh3.0 also showed larger fluorescence responses during hit trials than ACh2.0 ($\Delta F/F_0 = 5.93\%$ and 1.61% for ACh3.0 and ACh2.0, respectively) (Fig. 3l), in line with our observations in cultured cells and in flies. Overall, ACh3.0 allowed mapping of spatially heterogeneous release patterns of ACh across the S1 with subsecond resolution during sensorimotor discrimination.

Fig. 2 | Probing ACh dynamics in acute mouse brain slices and in vivo in *Drosophila*. a, Schematic illustration depicting the two-photon imaging of acute MHb–IPN brain slices prepared from mice expressing ACh2.0 or ACh3.0 in the IPN. A bipolar electrode placed in the IPN was used to evoke release of endogenous ACh. **b**, Pseudocolored images of the fluorescence response ($\Delta F/F_0$) of ACh2.0 and ACh3.0 to electrical stimuli (100 Hz for 5 s) in ACSF or 2 μM baclofen (Bac). The red dashed circles indicate the regions of interest (ROIs; 30 μm in diameter) used for quantification. Data are representative of 5–10 slices from 3–7 mice. **c**, Group summary of the fluorescence response of ACh2.0 and ACh3.0 to electrical stimuli at the indicated frequencies ($n = 11$ slices from 8 mice). The inset shows representative traces of ACh2.0 and ACh3.0 in response to 100-Hz electrical stimulation. **d**, Representative traces and group summary of the fluorescence response of ACh3.0 to electrical stimulation in either ACSF or the indicated drugs; $n = 5$ slices from 5 mice per group. Baclofen (Bac), 2 μM; saclofen (Sac), 100 μM; Tio, 10 μM. **e**, Representative traces and group summary of the fluorescence response of ACh3.0 to electrical stimulation in ACSF, 4-AP (100 μM) or 4-AP with Cd^{2+} (100 μM); $n = 5$ slices from 5 mice per group. **f**, Fluorescence traces of ACh3.0 in response to 100-ms electrical stimulation. The rise and decay phases of the fluorescence signals are fitted to a single-exponential function, and the time constants are summarized on the right; $n = 5$ slices from 5 mice per group. **g**, Pseudocolored images of the peak fluorescence response in the mushroom body horizontal lobe in transgenic flies expressing ACh2.0 or ACh3.0 during body shock (left), odorant application (middle) and perfusion with exogenous ACh (right). Similar results as the representative images were observed for more than five flies. **h**, Top, fluorescence traces measured in the mushroom body in transgenic flies expressing ACh2.0 (black) or ACh3.0 (red); where indicated, body shock, odorant stimulation or ACh perfusion was applied. Bottom, group summary of the fluorescence responses measured in the γ2 and γ3 lobes in the mushroom body; $n = 6$ flies per group; $P = 0.47$ for the comparison between γ2 and γ3 for ACh2.0 in response to shock, $P = 0.004$ for the comparison between γ2 and γ3 for ACh3.0 in response to shock, $P = 0.39$ for the comparison between γ2 and γ3 for ACh2.0 in response to odor, $P = 0.04$ for the comparison between γ2 and γ3 for ACh3.0 in response to odor, $P = 0.23$ for the comparison between γ2 and γ3 for ACh2.0 in response to ACh perfusion, $P = 0.61$ for the comparison between γ2 and γ3 for ACh3.0 in response to ACh perfusion. **i**, Left, schematic illustration depicting the experimental setup. CsChrimson–mCherry and ACh3.0 sensors were expressed in KCs in the mushroom body, and 635-nm laser light was used to activate cholinergic KCs. The fly brain was bathed in adult hemolymph-like solution (AHLS) containing 100 μM of the nicotinic ACh receptor blocker mecamylamine. 2PM, two-photon microscopy. Right, fluorescence images and pseudocolored images of the ACh3.0 sensor in response to 635-nm laser stimulation in the presence or absence of Tio (10 μM). Similar results as the representative images were observed for eight flies. **j**, Representative traces and group summary of the fluorescence response of ACh3.0 to the indicated number of 635-nm laser pulses applied at 10 Hz; $n = 8$ flies per group; $P = 0.006$. All data are shown as the mean ± s.e.m., with the error bars or shaded regions indicating s.e.m. Scale bars represent 50 μm (**b**) and 25 μm (**g** and **i**). Two-sided Student's t tests were performed in **h** and **j**: $^*P < 0.05$, $^{**}P < 0.01$; NS, not significant.

Finally, we expressed the ACh3.0 sensor in the mouse visual cortex and monitored the fluorescence signal using a miniature two-photon microscope attached to the head of the mouse[29] (Fig. 3m and Extended Data Fig. 9). During two-photon imaging, we placed the mouse on a treadmill and measured the ACh3.0 signal in response to auditory or visual stimuli or during the animal's locomotion. We observed a robust increase in ACh3.0 fluorescence when the mouse was running, but not during the application of visual or auditory stimuli (Fig. 3n). We could also identify spatially selective ACh signals at certain time points during running in a single imaging trial, indicating that ACh3.0 has high spatial and temporal resolution to resolve ACh patterns (Fig. 3o). Moreover, the fluorescence response positively correlated with the running speed of the mouse (Fig. 3p and Extended Data Fig. 9). The running-related increase in the ACh3.0 signal was abolished by the M_3R antagonist scopolamine, but not by the

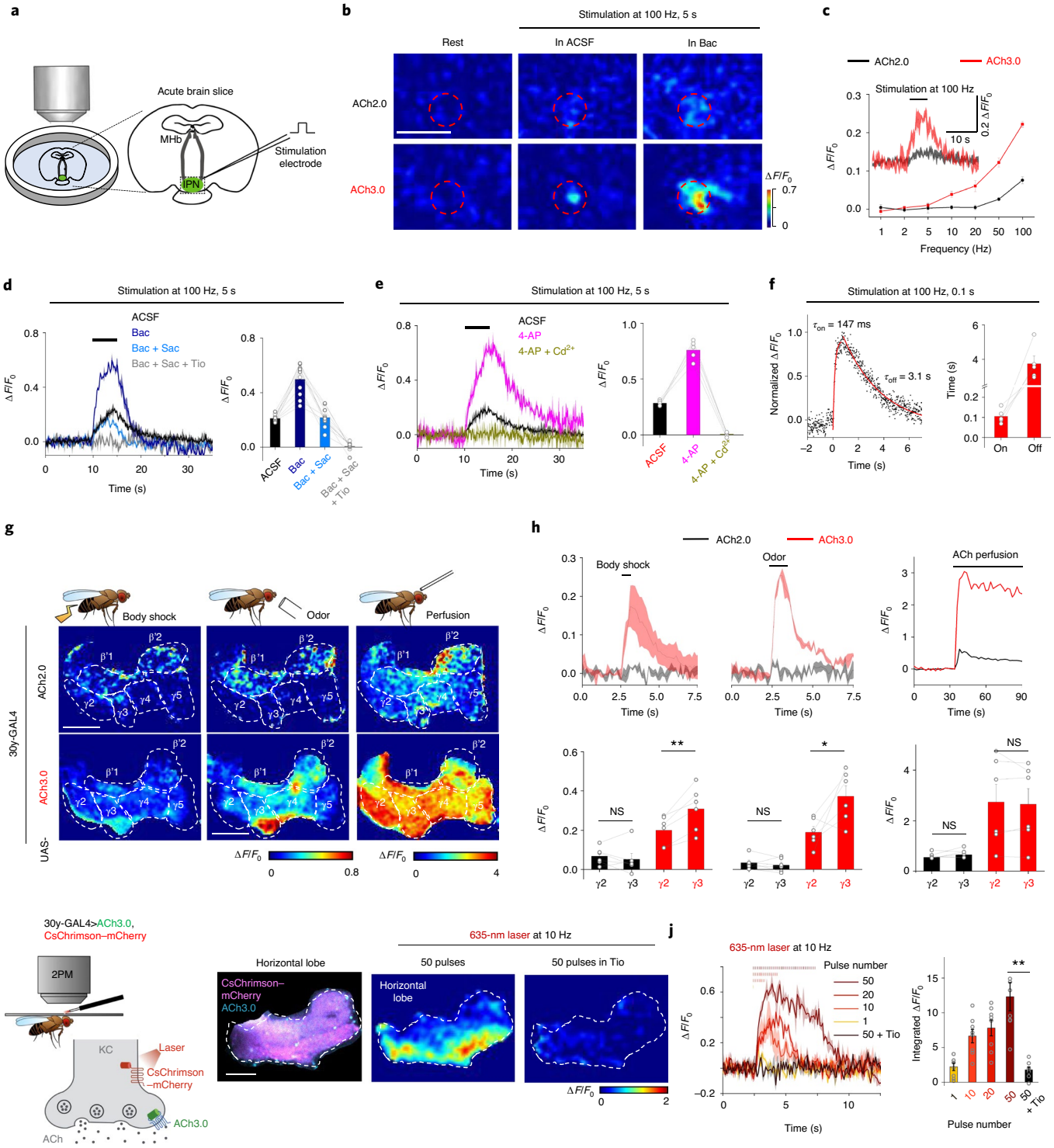

nicotinic ACh receptor blocker mecamylamine, indicating high specificity of the measured fluorescence signal (Extended Data Fig. 9).

Discussion

Here we here engineered $GRAB_{ACh3.0}$, which has higher sensitivity than $GRAB_{ACh2.0}$ while maintaining specificity, precise temporal

Fig. 3 | Monitoring in vivo ACh dynamics in mice. a, Top, schematic diagram depicting injection of an adeno-associated virus (AAV) encoding the ACh3.0 or ACh3.0-mut sensor into the BLA; the fluorescence response was recorded using fiber photometry. Bottom, fluorescence of the ACh3.0 sensor expressed in the BLA (left) and a cartoon illustration of the foot shock experiments (right). Scale bar, 200 μm. **b**, Pseudocolored fluorescence responses of ACh3.0 in the BLA to ten 0.2-s foot shock stimuli at 0.4 mA. Similar results as the representative result were observed for six mice. **c**, Representative traces and group summary of the fluorescence response of ACh3.0 in the BLA of mice following an intraperitoneal injection of saline (black), the AChEI donepezil (Done, red; 3 mg per kg body weight) or the M_3R antagonist scopolamine (Scop, gray; 6 mg per kg body weight). The average fluorescence response was calculated using the 1-s mean fluorescence after the initiation of foot shock ($n = 6$ mice per group); $P = 0.046$ for the comparison between saline and donepezil, $P = 0.0047$ for the comparison between donepezil and scopolamine, $P = 4 \times 10^{-5}$ for the comparison between saline and scopolamine. **d**, Similar to **c**, showing the fluorescence response of ACh3.0 and ACh3.0-mut to a 0.2-s foot shock; $n = 6$ and 4 mice for ACh3.0 and ACh3.0-mut, respectively; $P = 0.004$. **e**, Left, fluorescence images of ACh3.0 expressed in the BLA of control mice ($VAChT^{+/+}$, black) and mice with VAChT knockout in the forebrain ($VAChT^{-/-}$, blue). Middle and right, representative traces and group summary of the response measured in the BLA of $VAChT^{+/+}$ and $VAChT^{-/-}$ mice to 1-s foot shock; $n = 6$ mice per group; $P = 0.0008$. Scale bars represent 750 μm. **f**, Schematic diagram depicting injection of an AAV resulting in the expression of ACh3.0 or ACh3.0-mut into the mouse hippocampus (HPC); fluorescence was recorded in the mice during the sleep–wake cycle. The placement of intracranial EEG recording electrodes is also indicated. **g**, Representative recordings of EEG, EMG and ACh3.0 (top) or ACh3.0-mut (bottom) fluorescence response during the sleep–wake cycle. The mouse's asleep/awake status (awake, NREM sleep or REM sleep) was determined using the EEG and EMG data and is indicated. The s.d. of the signal during NREM sleep when there was no apparent fluctuation in the signal was used for normalization to calculate the normalized *z* score (see Methods for details). **h**, Left, group summary of the ACh3.0 fluorescence response (expressed as a normalized *z* score) in mice while awake and during NREM and REM sleep; $n = 5$ mice per group. Right, a comparison of the fluorescence response between ACh3.0 and ACh3.0-mut in the awake status ($n = 5$ mice for ACh3.0 and $n = 6$ mice for ACh3.0-mut) of mice. $P = 0.0025$ for the comparison between awake and NREM, $P = 0.045$ for the comparison between NREM and REM, $P = 0.19$ for the comparison between awake and REM, $P = 0.0009$ for the comparison between ACh3.0 and ACh3.0-mut. The comparison of ACh3.0 and ACh3.0-mut in other sleep status categories is summarized in Extended Data Fig. 8. **i**, Left, cartoon illustration of the head-fixed whisker-guided object localization task. Right, two-photon imaging of ACh sensors expressed in layer 2 of the S1 cortex. Scale bar, 100 μm. Similar results as the representative images were observed for three mice. **j**, Pseudocolored images showing representative fluorescence response of ACh3.0 on hit and correct rejection (CR) trials during the task, before and after intraperitoneal injection of scopolamine (5 mg per kg). Similar results as the representative images were observed for three mice. **k**, Average fluorescence response of ACh3.0 on hit and correct rejection trials, before and after scopolamine injection ($n = 3$ mice). **l**, Average fluorescence response comparing the ACh2.0 and ACh3.0 sensors on hit trials ($n = 3$ mice per group). **m**, Schematic illustration depicting the experiment in which mice expressing ACh3.0 in the visual cortex were placed on a treadmill and ACh3.0 fluorescence was recorded using a miniature two-photon microscope. **n**, Pseudocolored fluorescence response of ACh3.0 to an auditory stimulus (30 s of a 7,000-Hz tone; left), a visual stimulus (30 s of flashing light at 2 Hz; middle) or running on the treadmill (right). The responses of 30 consecutive trials were recorded and are plotted relative to the onset of each stimulus. **o**, Pseudocolored images showing the spatiotemporal distribution of ACh3.0 fluorescence during locomotion from a single trial. R1, R2 and R3 are three representative ROIs (40 μm in diameter) indicating spatially selective ACh signals at the indicated time point during running. The averaged fluorescence signal during the entire running process is also shown. Scale bar, 50 μm. Similar results as the representative images were observed for five mice. **p**, Representative traces of ACh3.0 fluorescence in mice recorded while running on a treadmill at the indicated speeds; each trace was averaged from ten trials. All data are shown as the mean ± s.e.m., with the error bars or shaded regions indicating s.e.m. Two-sided Student's *t* tests were performed in **c**–**e** and **h**: $^{*}P < 0.05$, $^{**}P < 0.01$, $^{***}P < 0.001$; NS, not significant.

and spatial resolution, and high photostability in detecting ACh. The improved sensor provides a robust tool for testing hypotheses about the dynamics of cholinergic activity under both physiological and pathophysiological conditions. With respect to studying physiological processes, the ACh3.0 sensor allows the real-time visualization of compartment-specific ACh release in the *Drosophila* olfactory system and cholinergic dynamics during the sleep–wake cycle in mice, shedding light on how cholinergic signaling is regulated. The improved ACh sensor, together with other GPCR-based neurotransmitter sensors recently developed[8,30–34], should help to address fundamental biological questions on neuromodulation in the future.

Online content

Any methods, additional references, Nature Research reporting summaries, source data, extended data, supplementary information, acknowledgements, peer review information; details of author contributions and competing interests; and statements of data and code availability are available at https://doi.org/10.1038/s41592-020-0953-2.

Received: 3 November 2019; Accepted: 11 August 2020;
Published online: 28 September 2020

References

1. Dale, H. H. The action of certain esters and ethers of choline, and their relation to muscarine. *J. Pharmacol. Exp. Ther.* **6**, 147–190 (1914).
2. Hasselmo, M. E. The role of acetylcholine in learning and memory. *Curr. Opin. Neurobiol.* **16**, 710–715 (2006).
3. Winkler, J., Suhr, S., Gage, F., Thal, L. & Fisher, L. Essential role of neocortical acetylcholine in spatial memory. *Nature* **375**, 484–487 (1995).
4. Krnjević, K. & Miledi, R. Acetylcholine in mammalian neuromuscular transmission. *Nature* **182**, 805–806 (1958).
5. Magleby, K. L. & Stevens, C. F. A quantitative description of end-plate currents. *J. Physiol.* **223**, 173–197 (1972).
6. Marrosu, F. et al. Microdialysis measurement of cortical and hippocampal acetylcholine release during sleep–wake cycle in freely moving cats. *Brain Res.* **671**, 329–332 (1995).
7. Nguyen, Q.-T. et al. An in vivo biosensor for neurotransmitter release and in situ receptor activity. *Nat. Neurosci.* **13**, 127–132 (2010).
8. Jing, M. et al. A genetically encoded fluorescent acetylcholine indicator for in vitro and in vivo studies. *Nat. Biotechnol.* **36**, 726–737 (2018).
9. Zhang, X., Noyes, N. C., Zeng, J., Li, Y. & Davis, R. L. Aversive training induces both presynaptic and postsynaptic suppression in *Drosophila*. *J. Neurosci.* **39**, 9164–9172 (2019).
10. Zhu, P. K. et al. Nanoscopic visualization of restricted nonvolume cholinergic and monoaminergic transmission with genetically encoded sensors. *Nano Lett.* **20**, 4073–4083 (2020).
11. Tautermann, C. S. et al. Molecular basis for the long duration of action and kinetic selectivity of tiotropium for the muscarinic M3 receptor. *J. Med. Chem.* **56**, 8746–8756 (2013).
12. Disse, B. et al. Ba 679 BR, a novel long-acting anticholinergic bronchodilator. *Life Sci.* **52**, 537–544 (1993).
13. Falkenburger, B. H., Jensen, J. B. & Hille, B. Kinetics of M1 muscarinic receptor and G protein signaling to phospholipase C in living cells. *J. Gen. Physiol.* **135**, 81–97 (2010).
14. Ziegler, N., Bätz, J., Zabel, U., Lohse, M. J. & Hoffmann, C. FRET-based sensors for the human M1-, M3-, and M5-acetylcholine receptors. *Bioorg. Med. Chem.* **19**, 1048–1054 (2011).

15. Wan, Q. et al. Mini G protein probes for active G protein-coupled receptors (GPCRs) in live cells. *J. Biol. Chem.* **293**, 7466–7473 (2018).
16. Barnea, G. et al. The genetic design of signaling cascades to record receptor activation. *Proc. Natl Acad. Sci. USA* **105**, 64–69 (2008).
17. Dana, H. et al. Sensitive red protein calcium indicators for imaging neural activity. *eLife* **5**, e12727 (2016).
18. Zhang, J. et al. Presynaptic excitation via $GABA_B$ receptors in habenula cholinergic neurons regulates fear memory expression. *Cell* **166**, 716–728 (2016).
19. Yao Yang, M., Armstrong, J. D., Vilinsky, I., Strausfeld, N. J. & Kaiser, K. Subdivision of the *Drosophila* mushroom bodies by enhancer-trap expression patterns. *Neuron* **15**, 45–54 (1995).
20. Klapoetke, N. C. et al. Independent optical excitation of distinct neural populations. *Nat. Methods* **11**, 338–346 (2014).
21. Vazquez, J. & Baghdoyan, H. A. Basal forebrain acetylcholine release during REM sleep is significantly greater than during waking. *Am. J. Physiol. Regul. Integr. Comp. Physiol.* **280**, R598–R601 (2001).
22. Picciotto, M. R., Higley, M. J. & Mineur, Y. S. Acetylcholine as a neuromodulator: cholinergic signaling shapes nervous system function and behavior. *Neuron* **76**, 116–129 (2012).
23. Jiang, L. et al. Cholinergic signaling controls conditioned fear behaviors and enhances plasticity of cortical–amygdala circuits. *Neuron* **90**, 1057–1070 (2016).
24. Li, X. et al. Generation of a whole-brain atlas for the cholinergic system and mesoscopic projectome analysis of basal forebrain cholinergic neurons. *Proc. Natl Acad. Sci. USA* **115**, 415–420 (2018).
25. Seltzer, B. Donepezil: a review. *Expert Opin. Drug Metab. Toxicol.* **1**, 527–536 (2005).
26. Martins-Silva, C. et al. Novel strains of mice deficient for the vesicular acetylcholine transporter: insights on transcriptional regulation and control of locomotor behavior. *PLoS ONE* **6**, e17611 (2011).
27. Xu, M. et al. Basal forebrain circuit for sleep–wake control. *Nat. Neurosci.* **18**, 1641–1647 (2015).
28. Cheung, J., Maire, P., Kim, J., Sy, J. & Hires, S. A. The sensorimotor basis of whisker-guided anteroposterior object localization in head-fixed mice. *Curr. Biol.* **29**, 3029–3040 (2019).
29. Zong, W. et al. Fast high-resolution miniature two-photon microscopy for brain imaging in freely behaving mice. *Nat. Methods* **14**, 713–719 (2017).
30. Patriarchi, T. et al. Ultrafast neuronal imaging of dopamine dynamics with designed genetically encoded sensors. *Science* **360**, eaat4422 (2018).
31. Feng, J. et al. A genetically encoded fluorescent sensor for rapid and specific in vivo detection of norepinephrine. *Neuron* **102**, 745–761 (2019).
32. Liang, R., Broussard, G. J. & Tian, L. Imaging chemical neurotransmission with genetically encoded fluorescent sensors. *ACS Chem. Neurosci.* **6**, 84–93 (2015).
33. Jing, M., Zhang, Y., Wang, H. & Li, Y. G-protein-coupled receptor-based sensors for imaging neurochemicals with high sensitivity and specificity. *J. Neurochem.* **151**, 279–288 (2019).
34. Sun, F. et al. A genetically encoded fluorescent sensor enables rapid and specific detection of dopamine in flies, fish, and mice. *Cell* **174**, 481–496 (2018).

Methods

Animals. Male and female postnatal day (P) 0 Sprague–Dawley rats were used to prepare cultured cortical neurons; P28–P48 wild-type C57BL/6N mice were used to prepare the acute brain slices and for two-photon in vivo imaging. C57BL/6J mice were used for fiber photometry recording. Mice lacking VAChT in the forebrain were generated as previously described[35] by crossing *VAChT*$^{flox/flox}$ mice (Chat/Slc18a3$^{tm1.2Vpra}$ mice generated on a mixed C57BL/6J×129/SvEv background, backcrossed to C57BL/6J mice for ten generations) with *Nkx2.1*-Cre mice (The Jackson Laboratory, stock no. JAX008661), yielding VAChT$^{-/-}$ offspring and control (*VAChT*$^{flox/flox}$) littermates (referred to here as VAChT$^{+/+}$). All rodents were either family or pair housed in a temperature-controlled room with a 12-h light/12-h dark cycle. All procedures for animal surgery and experimentation were performed using protocols approved by the Animal Care and Use Committees at the Chinese Institute for Brain Research, the Peking University, the Chinese Academy of Sciences (CAS), Huazhong University of Science and Technology, the University of Southern California (20732-009) and the University of Western Ontario (2016-104) and were performed in accordance with the guidelines established by the US National Institutes of Health. To generate transgenic *Drosophila*, the plasmids 10xUAS-IVS-ACh3.0-p10 and 10xLexAop2-IVS-ACh3.0-p10 were constructed and integrated into attp40 or VK00005 in the fly genome mediated by PhiC31. The embryo injections were performed at the Core Facility of *Drosophila* Resource and Technology, Shanghai Institute of Biochemistry and Cell Biology, CAS. Transgenic flies were raised on conventional cornmeal at 25 °C, with ~70% humidity, under a 12-h light/12-h dark cycle. The fly lines used in this study were as follows: 30y-GAL4 (BDSC, 30818) from Y. Rao (Peking University), UAS-CsChrimson–mCherry and UAS-jRCaMP1a (BDSC, 64427) from C. Zhou (Institute of Zoology, CAS) and MB247-LexA from Y. Zhong (Tsinghua University).

Molecular biology. Plasmids were generated using the Gibson assembly method[36]. DNA fragments were generated by PCR amplification using primers (Thermo Fisher Scientific) with 30-bp overlap. The fragments were then assembled using T5 exonuclease (New England Biolabs), Phusion DNA polymerase (Thermo Fisher Scientific) and Taq ligase (iCloning). All sequences were verified by Sanger sequencing at the Sequencing Platform in the School of Life Sciences of Peking University. For screening in HEK293T cells, the ACh sensor constructs were cloned into the pDisplay vector (Invitrogen) followed by the IRES-mCherry–CAAX sequence, which served as a membrane marker to calibrate the signal intensity. Site-directed mutagenesis of the linker sequences and residues in cpEGFP was performed using primers containing randomized NNB codons (48 codons in total, encoding all 20 amino acids; Thermo Fisher Scientific). For AAV construction, the sequences encoding the ACh3.0 sensor and the mutant ACh3.0-mut sensor were cloned into an AAV vector under the control of the human synapsin (*SYN1*) promoter. To generate transgenic *Drosophila* lines, the sequence encoding the ACh3.0 sensor was cloned into the pJFRC28 vector, which was then used to generate transgenic flies via PhiC31-mediated site-directed integration into attp40.

Cell culture, transfection and imaging. HEK293T cells (ATCC cell line CRL-3216) were cultured at 37 °C in 5% CO_2 in DMEM (Gibco) supplemented with 10% (vol/vol) FBS (Gibco) and 1% penicillin-streptomycin (Gibco). HEK293 cells stably expressing a tTA-dependent luciferase reporter and a β-arrestin2–TEV fusion construct were a gift from B.L. Roth (University of North Carolina). Rat cortical neurons were prepared from P0 Sprague–Dawley rat pups (both male and female; Beijing Vital River). In brief, the brains were dissected, and cortical neurons were dissociated in 0.25% trypsin–EDTA (Gibco), plated on 12-mm glass coverslips coated with poly(D-lysine) (Sigma-Aldrich) and cultured at 37 °C in 5% CO_2 in neurobasal medium containing 2% B-27 supplement, 1% GlutaMAX and 1% penicillin-streptomycin (all from Gibco). HEK293T cells were transfected using the polyethylenimine (PEI) method (with a typical ratio of 1 μg DNA to 4 μg PEI); the medium was replaced 4–6 h later, and cells were imaged 24 h after transfection. Cultured neurons were transfected at 7–9 d in vitro using the calcium phosphate transfection method, and experiments were performed 48 h after transfection. For screening of candidate sensors, cultured HEK293T cells expressing the various candidate sensors were first imaged using the Opera Phenix High-Content Screening System (PerkinElmer) equipped with a ×60/1.15-NA water-immersion objective, a 488-nm laser and a 561-nm laser; the ACh sensor's signal was obtained using a 525/50-nm emission filter, and the mCherry–CAAX signal was obtained using a 600/30-nm emission filter. The ratio between green (G) and red (R) fluorescence was calculated before and after application of 100 μM ACh, and the change in the G/R ratio was used as the fluorescence response; the peak G/R ratio was used as a brightness index. Candidate sensors with the best performance were subsequently imaged using a Ti-E A1 inverted confocal microscope (Nikon) equipped with a ×40/1.35-NA oil-immersion objective, a 488-nm laser and a 561-nm laser. Drugs were prepared in Tyrode's solution containing (in mM) 150 NaCl, 4 KCl, 2 $MgCl_2$, 2 $CaCl_2$, 10 HEPES and 10 glucose (pH 7.4) and perfused into the imaging chamber. The ACh sensor's signal was obtained using a 525/50-nm emission filter, and the mCherry signal was obtained using a 595/50-nm emission filter. Cultured neurons expressing the ACh sensor were similarly imaged using the inverted confocal microscope with drugs added by perfusion. To measure the kinetics of the ACh3.0 sensor, the confocal line scanning mode (2,600 Hz) was used to record the fluorescence response when cells were locally puffed with different concentrations of ACh in the pipette. The dose-dependent relationship between fluorescence response and ACh concentration in line scanning mode was further calibrated by bath application of ACh at different concentrations. The maximum fluorescence response at the steady state after local ACh puffing was used to estimate the real local ACh concentration reaching the cell. The estimated local ACh concentration and the time constant of the fluorescence response were used to calculate the association rate constant between ACh3.0 and ACh. Similarly, the decay kinetics were measured by locally puffing cells with the Tio antagonist while they were bathed in ACh, and the disassociation rate constant was calculated as $1/\tau_{off}$.

Slice preparation and imaging. AAVs expressing either ACh2.0 or ACh3.0 were packaged by Vigene Biosciences and were injected into the mouse IPN (500 nl per mouse, titer of 1×10^{13} viral genomes per ml). Two weeks after virus injection, the animals were anesthetized with an intraperitoneal injection of Avertin (250 mg per kg body weight), and the heart was perfused with 5 ml slicing buffer containing (in mM) 110 choline chloride, 2.5 KCl, 1.25 NaH_2PO_4, 25 $NaHCO_3$, 7 $MgCl_2$, 25 glucose and 2 $CaCl_2$. The mice were then decapitated, and brains were removed immediately and placed directly in cold oxygenated slicing buffer. The brains were first blocked at a ~45° angle relative to the horizontal plane and then sectioned into 250-μm-thick slices using a VT1200 vibratome (Leica); the sections were transferred to oxygenated Ringer's buffer containing (in mM) 125 NaCl, 2.5 KCl, 1.25 NaH_2PO_4, 25 $NaHCO_3$, 1.3 $MgCl_2$, 25 glucose and 2 $CaCl_2$. The slices were then recovered at 34 °C for at least 40 min. For two-photon fluorescence imaging, slices were transferred to an imaging chamber and placed in an FV1000MPE two-photon microscope (Olympus) equipped with a ×40/0.80-NA water-immersion objective and a mode-locked Mai Tai Ti:Sapphire laser (Spectra-Physics) tuned to 920 nm for excitation and a 495- to 540-nm filter for signal collection. For electrical stimulation, a bipolar electrode (WE30031.0A3, MicroProbes) was positioned near the IPN region under fluorescence guidance, and imaging and stimulation were synchronized using an Arduino board with a custom program. The stimulation voltage was set at ~4 V, and the duration of each stimulation pulse was set at 1 ms. Drugs were added by perfusion or were applied by bath.

Two-photon imaging in *Drosophila*. Female *Drosophil*a within 3 weeks of eclosion were used for imaging experiments. The fly was mounted on a customized chamber by tape, such that the antennae and abdomen were exposed to the air. The cuticle between the compound eyes, as well as the air sacs and fat bodies, were removed to expose the brain, which was then bathed in saline (AHLS) containing (in mM) 108 NaCl, 5 KCl, 5 HEPES, 5 trehalose, 5 sucrose, 26 $NaHCO_3$, 1 NaH_2PO_4, 2 $CaCl_2$ and 2 $MgCl_2$. The same Olympus two-photon microscope as well as the electrical stimulation equipment used for brain slice imaging was also used here. A 920-nm laser was used for excitation. A 495- to 540-nm filter was used for ACh2.0 or ACh3.0 imaging, and a 575- to 630-nm filter was used for jRCaMP1a imaging. For odor stimulation, the odorant isoamyl acetate (Sigma-Aldrich, 306967) was first diluted 200-fold in mineral oil in a bottle and was then diluted 5-fold in air. The odorant was then delivered to the fly's antennae at a rate of 1,000 ml min^{-1}. For body shock, two wires were attached to the abdomen of the fly, and an electrical pulse of 60–80 V was delivered for 500 ms during stimulation. For ACh application, a patch of the blood–brain barrier of the fly was carefully removed with tweezers before imaging and saline containing ACh was delivered to the brain to a 20 mM final concentration. For optogenetic stimulation, the 635-nm laser was used to deliver pulses (1-ms pulses at 10 Hz) through optical fibers placed near the fly's brain. Flies were fed with cornmeal containing 10 μM β-carotene (Sigma-Aldrich) 3 d before optogenetics experiments. For electrical stimulation, a glass electrode (resistance of ~0.2 MΩ) was placed in the region of the mushroom bodies and the stimulation voltage was set at 20–80 V. Tio was added directly to the saline to a final concentration of 10 μM, and the following experiments were performed 10 min after application. The nicotinic ACh receptor blocker mecamylamine (100 μM) was bath applied in electrical stimulation and optogenetic stimulation experiments. The sampling rates of imaging were set at 7 Hz during odor or body shock stimulation, 0.5 Hz during ACh application, 10 Hz during optogenetic stimulation and 12 Hz during electrical stimulation. Arduino was used to synchronize stimulation delivery and imaging with a custom program.

Fiber photometry, EEG and EMG recordings in mice. The AAV encoding ACh3.0 was injected into the BLA (AP, –1.4 mm; ML, 3.1 mm; DV, 4.1 mm) with a microsyringe pump or into the hippocampus dorsal CA1 (AP, –2.2 mm; ML, 1.5 mm; DV, 1.2 mm) using a Nanoject II (Drummond Scientific) via a glass pipette. An optic fiber (230 μm, 0.37 NA or 400 μm, 0.48 NA for BLA recording; 200 μm, 0.39 NA for hippocampus recording) was inserted into the same coordinates used for virus injection. For the recording in BLA, the f-Scope fiber photometry system (BiolinkOptics) with laser power adjusted to 20–30 μW or the fiber photometry system from Doric Lenses with the power for the 465-nm LED set at 20–25 μW was used to record fluorescence signals. For recording in the hippocampus, an optic fiber (Thorlabs, FT200UMT) was attached to the implanted ferrule via a ceramic sleeve and recorded emission fluorescence using fiber

photometry. The photometry rig was constructed using parts from Doric Lenses, including a fluorescence optical minicube (FMC4_AE(405)_E(460-490)_F(500-550)_S), a blue LED (CLED_465), an LED driver (LED_2) and a photoreceiver (NPM_2151_FOA_FC). For recordings containing an isosbestic channel (405 channel), we used a fluorescence optical minicube (FMC4_IE(400-410)_E(460-490)_F(500-550)_S), a blue LED (CLED_465), a deep-blue LED (CLED_405), an LED driver (LED_2) and two photoreceivers (NPM_2151_FOA_FC). During recording, a software-controlled locked-in detection algorithm was implemented in the TDT RZ2 system using the fiber photometry 'Gizmo' module of Synapse software (modulation frequency: 459 Hz for single-channel recording and 271 or 459 Hz for the second channel in two-channel mode; low-pass filter for demodulated signal: 20 Hz, sixth order). The intensity of the excitation light was measured as 10–20 µW from the tip of the optical fiber. The photometry data were stored using a sampling frequency of 1,017 Hz. Data collected by the Quebec system were first filtered using a 6-Hz low-pass filter and analyzed. Raw data from the hippocampus recordings were first binned at 1 Hz and the background autofluorescence was subtracted. We calculated $\Delta F/F_0$ using a baseline obtained by fitting the autofluorescence-subtracted data with a second-order exponential function. To identify fast components or remove the slow drift of the photometry signal, we used a MATLAB script 'BEADS' with a cutoff frequency of 0.0005 cycles per sample (https://www.mathworks.com/matlabcentral/fileexchange/49974-beads-baseline-estimation-and-denoising-with-sparsity). To reduce artifacts induced by movement or hemodynamic change, we scaled the signal for the 405 channel to the best-fit signal for the green channel using linear regression and then subtracted the scaled signal from the green signal to obtain the artifact-corrected recording. To quantify the change in the photometry signal across multiple animals or conditions, the z-score-transformed $\Delta F/F_0$ was further normalized using the s.d. of the signal during NREM sleep when there was no apparent fluctuation in the signal. The normalized z score was used for all analyses in the sleep–wake recordings.

To implant EEG and EMG recording electrodes, mice were anesthetized with isoflurane (5% induction; 1.5–2% maintenance) and placed on a stereotaxic frame with a heating pad. Two stainless steel screws for EEG were inserted into the skull above the visual cortex, two other screws were inserted into the skull above the frontal cortex, two insulated EMG electrodes were inserted into the neck muscle and a reference electrode was attached to a screw inserted into the skull above the cerebellum. The implant was secured to the skull with dental cement. All experiments were carried out at least 1 week after the surgery. The EEG and EMG signals were recorded using TDT System-3 amplifiers (RZ2 + PZ5) with a high-pass filter at 0.5 Hz and digitized at 1,500 Hz. Spectral analysis was carried out using fast Fourier transform (FFT) with a frequency resolution of 0.18 Hz. The brain states were scored every 5 s semiautomatically using a MATLAB GUI and were validated manually by trained experimenters. Awake was defined as desynchronized EEG and high EMG activity; NREM sleep was defined as synchronized EEG with high-amplitude delta activity (0.5–4 Hz) and low EMG activity; and REM sleep was defined as high power at theta frequencies (6–9 Hz) and low EMG activity.

For ACh recording during foot shock, mice were first habituated to the behavioral chamber set at a background noise level of 65 dB and under infrared light for video visualization for four sessions (10 min per session, twice per day). Then, mice were habituated for 5 min before receiving foot shock stimuli (10 trials of 0.2 s or 1 s in length, foot shock intensity of 0.4 mA, inter-trial intervals of 20 s). Each foot shock was coupled to the delivery of a 10-ms-long TTL output for synchronization with the fiber photometry recordings.

Two-photon imaging in mice. To express ACh3.0, the mice were initially anesthetized with an injection of Avertin or isoflurane (3% induction; 1–1.5% maintenance), the skin was retracted from the head and a metal recording chamber was affixed. On the second day, the mice were anesthetized again, the skull above the visual cortex was opened and ~400–500 nl of AAV was injected at a depth of 0.5 mm. A 2 mm × 2 mm or 4 mm × 4 mm square coverslip was used to replace the skull. For imaging in the barrel cortex, all whiskers except C2 were trimmed before ISI and remained trimmed throughout the experiments, and mice were water restricted for around 1 week after the cranial window surgery. After cranial window surgery, mice were put on a whisker-guided go/no-go location task while undergoing two-photon imaging in the barrel cortex. During the behavior, mice explored a presented pole with a whisker during the sampling period. During the answer period, mice licked for a water reward when the pole was proximal (hit trials) and withheld licking when the pole was distal (correct rejection trials). Two-photon imaging using a miniature microscope in the visual cortex was performed 3 weeks after virus injection. In brief, the mice first had the baseplate attached and were allowed to habituate for 2–3 d before the experiment. During the experiment, the miniature two-photon microscope was placed on the baseplate, and the mice were head-fixed on a treadmill controlled by an electric motor. The output trigger from the computer was used to synchronize the imaging with the treadmill. The speed of the treadmill was adjusted by the motor and was calibrated. Visual and auditory stimuli were generated using MATLAB. The visual stimulation was delivered to the mice by a video screen placed ~30 cm from the contralateral eye relative to the virus-expressing hemisphere. The visual and auditory stimuli were synchronized with the imaging using an Arduino board. Where indicated, drugs were injected intraperitoneally 30 min before the experiment.

Immunohistochemistry and immunofluorescence. Immunohistochemistry was performed as previously described[37]. In brief, the mice were anesthetized, the heart was perfused and the brain was extracted and postfixed overnight in 4% paraformaldehyde. The fixed brains were then transferred to a PBS–azide solution, and a vibratome was used to cut 45-µm sections. After slicing, free-floating sections were rinsed in washing buffer (PBS containing 0.15% Triton X-100), preincubated in 1% hydrogen peroxide for 30 min and then rinsed in washing buffer. Sections were blocked for 1 h in washing buffer containing 5% (wt/vol) BSA and 5% (vol/vol) normal goat serum. After blocking, the sections were incubated overnight in washing buffer containing rabbit anti-VAChT antibody (Synaptic Systems, 139103; 1:250) and 2% normal goat serum. After overnight incubation in primary antibody, the sections were rinsed in washing buffer and then incubated for 1 h in biotinylated anti-rabbit antibody (Vector Laboratories, ba-9400; 1:200) in washing buffer containing 2% normal goat serum. The sections were rinsed in washing buffer and incubated with the VECTASTAIN ABC kit (Vector Laboratories) in accordance with the manufacturer's instructions. The substrate diaminobenzidine (Vector Laboratories) was added as a chromogen, and the sections where counterstained with 0.5% methyl green solution. The sections were then cleared in xylene and mounted on glass slides. For immunofluorescence, slices were prepared as described above and incubated in Tris-buffered saline (TBS) containing 1.2% Triton X-100 for 20 min. The sections were rinsed with TBS and blocked for 1 h in TBS containing 5% (vol/vol) normal goat serum. After blocking, the sections were rinsed twice with TBS and then incubated for 24 h at 4 °C with chicken anti-GFP (Abcam, ab13970; 1:500) in TBS containing 0.2% Triton X-100 and 2% normal goat serum. After 24 h, the sections were washed twice for 10 min each in TBS. The sections were then incubated for 1 h in Alexa Fluor 488-conjugated goat anti-chicken antibody (Life Technologies, A11039; 1:500) in TBS containing 0.2% Triton X-100 and 2% normal goat serum. The sections were washed twice in TBS for 10 min each and then incubated in Hoechst 33342 (Thermo Fisher, H3570; 1:500) to counterstain the nuclei. The EVOS FL Auto 2 Cell Imaging System (Invitrogen) was used to visualize the sections.

Statistics and reproducibility. Except where indicated otherwise, all summary data are reported as the mean ± s.e.m. Imaging data were processed with ImageJ (1.49V) or MATLAB software (matlab2013) and were plotted with Origin 9.1 (Originlab). The SNR was calculated as the peak response divided by the s.d. of the baseline fluorescence. Group differences were analyzed using the two-sided Student's t test, and differences with $P < 0.05$ were considered significant. For all representative images and traces, similar results were obtained for more than five independent experiments.

Reporting Summary. Further information on research design is available in the Nature Research Reporting Summary linked to this article.

Data availability

The plasmids pAAV-hsyn-ACh3.0 and pAAV-hsyn-DIO-ACh3.0 have been deposited to Addgene (121922 and 121933) and are available. The transgenic *Drosophila* and related materials have been deposited to the Bloomington Drosophila Stock Center (flies: FBti0210605, FBti0210606, FBti0210607 and FBti0210608; plasmids: FBtp0140745, FBtp0140746, FBtp0140747 and FBtp0140748) and are available. Source data are provided with this paper.

Code availability

The custom-written MATLAB, Arduino and TDT programs will be provided upon request.

References

35. Al-Onaizi, M. A. et al. Regulation of cognitive processing by hippocampal cholinergic tone. *Cereb. Cortex* **27**, 1615–1628 (2017).
36. Gibson, D. G. et al. Enzymatic assembly of DNA molecules up to several hundred kilobases. *Nat. Methods* **6**, 343–345 (2009).
37. Janickova, H. et al. Selective decrease of cholinergic signaling from pedunculopontine and laterodorsal tegmental nuclei has little impact on cognition but markedly increases susceptibility to stress. *FASEB J.* **33**, 7018–7036 (2019).

Acknowledgements

We thank Y. Rao (Peking University) for generously sharing a two-photon microscope and X. Lei (Peking University) for providing support of the Opera Phenix High-Content Screening System at PKU–CLS. We thank W. Inoue (University of Western Ontario) for kindly sharing the Multi Conditioning System foot-shocker. Work at the University of Western Ontario was supported by the Canada First Research Excellence Fund (CFREF; to L.M.S., V.F.P., T.J.B. and M.A.M.P.) and CIHR (PJT 159781 to V.F.P.). O.K. was supported by an OGS PhD Fellowship and the Jonathan and Joshua Graduate

Scholarship. M.S. was supported by CFREF. This work was supported by the General Research Program of the National Natural Science Foundation of China (projects 31671118 to Yulong Li and 31327901 to H.C.), the NIH BRAIN Initiative (grant U01NS103558 to Yulong Li), the Beijing Brain Initiative of the Beijing Municipal Science & Technology Commission (Z181100001518004 to Yulong Li), the Junior Thousand Talent Program of China and grants from the Peking–Tsinghua Center for Life Sciences and the State Key Laboratory of Membrane Biology at the Peking University School of Life Science (to Yulong Li).

Author contributions

M.J. and Yulong Li conceived the project. Yuexuan Li, S.Z., T.Q. and M.J. screened the candidate ACh sensors and characterized the sensors in cultured cells and brain slices. J. Zeng and K.T. performed the experiments with transgenic flies. W.P. performed the fiber photometry recordings of ACh signals during the sleep–wake cycle under the supervision of M.X. P.H. performed the fiber photometry recordings of foot-shock-induced ACh signals in the BLA under the supervision of H.L. M.S. and O.K. performed the recordings in VAChT$^{-/-}$ mice under the supervision of L.M.S., V.F.P., T.J.B. and M.A.M.P. S.P. performed the luciferase complementation assay. M.J. and R.W. performed the ACh imaging experiments in the visual cortex using miniature two-photon microscopy under the supervision of L.C. and H.C. J. Zou and S.T. performed imaging in the barrel cortex with the supervision of S.A.H. All authors contributed to the data analysis. M.J. and Yulong Li wrote the manuscript with input from all other authors.

Competing interests

M.J. and Yulong Li have filed patent applications, the value of which could be affected by this publication.

Additional information

Extended data is available for this paper at https://doi.org/10.1038/s41592-020-0953-2.

Supplementary information is available for this paper at https://doi.org/10.1038/s41592-020-0953-2.

Correspondence and requests for materials should be addressed to M.J. or Y.L.

Peer review information Nina Vogt was the primary editor on this article and managed its editorial process and peer review in collaboration with the rest of the editorial team.

Reprints and permissions information is available at www.nature.com/reprints.

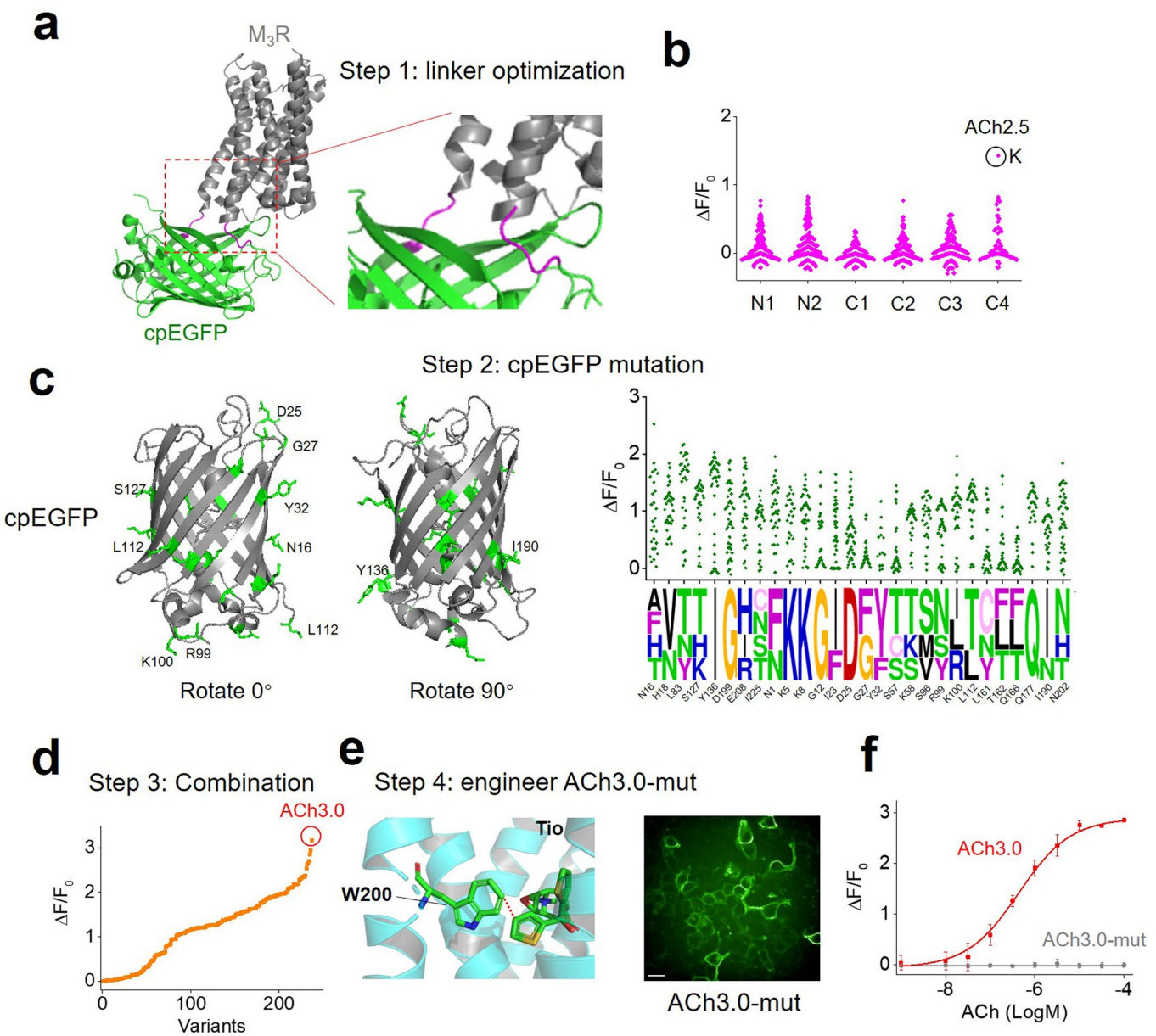

Extended Data Fig. 1 | The engineering process leading to the GRAB$_{ACh3.0}$ sensor. a, Schematic illustration depicting the predicted structure of the generic GRAB$_{ACh}$ sensor, with the linker region between the receptor (M_3R) and cpEGFP magnified at the right and shown in magenta. The crystal structures are from protein database (PDB) archive (PDB ID: 4DAJ for M_3R; PDB ID: 3EK4 for cpGFP). **b**, Site-directed mutagenesis of residues in the N and C termini of the linker region. The numbers indicate amino acid positions in the linker region (the first on N-terminus as N1, and the first on C-terminus as C1). The candidate with the best response is shown in a black circle and is called ACh2.5, with the C4 residue mutated to K; this candidate is used for further engineering steps. **c**, Left: crystal structure of the cpEGFP moiety in the ACh3.0 sensor; targeted residues for mutagenesis screening are indicated in green and the corresponding amino acid labeled on the structure. Right, the fluorescence response of the indicated mutant candidate sensors is shown on top, with the sequences of the best-performing candidates on the bottom; the relative size of each letter reflects the probability of that amino acid in the sequence. The residues are named by the amino acid followed by the position in cpGFP (the first amino acid in cpGFP as N1). The crystal structures are from protein database (PDB) archive (PDB ID: 3EK4 for cpGFP). **d**, The fluorescence response of each candidate ACh sensor with combined mutations from the best-performing sites in the linker and cpEGFP. Each point is calculated from the average of >100 cells. **e**, left, illustration of the ligand binding pocket in M_3R, which was mutated from W to A. Right, fluorescence image of HEK293T cells expressing ACh3.0-mut. **f**, The fluorescence response of ACh3.0 and ACh3.0-mut to indicated concentration of ACh applied (n = 3 wells for each point, with each well averaging >100 cells). Scale bar represents 10 μm. All data are shown as mean value ± SEM, with the error bars or shaded regions indicating SEM.

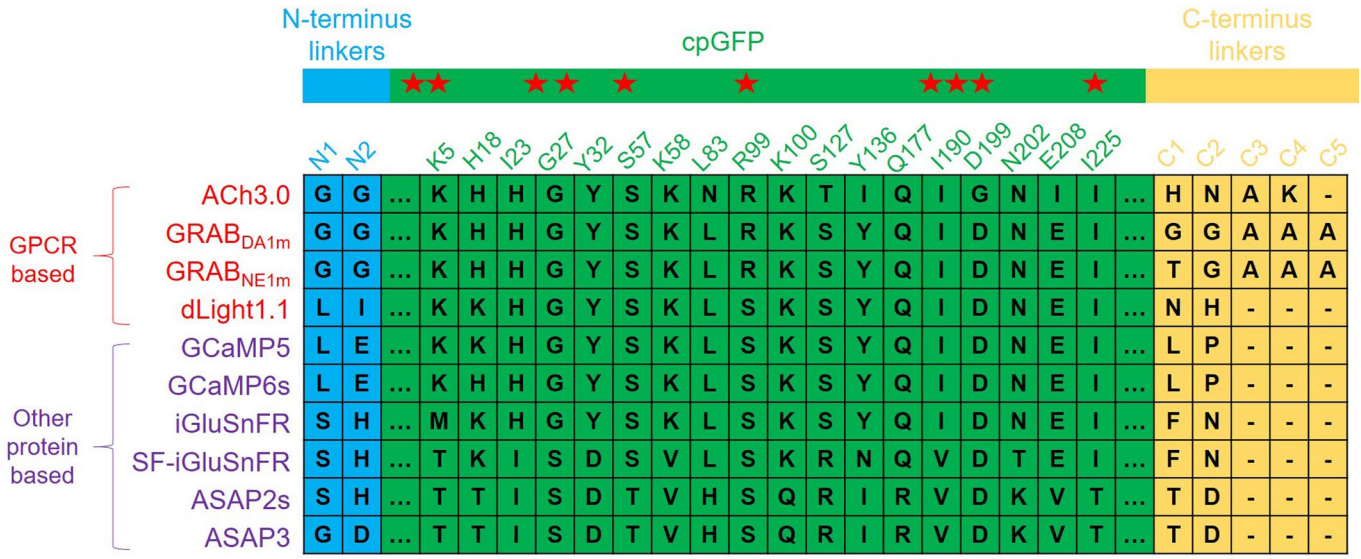

Extended Data Fig. 2 | Amino acid sequences of different cpGFP-based sensors. The summary of amino acids in linkers and critical residues within cpGFP in different genetically encoded sensors, including GPCR-based sensors and other protein backbone-based sensors.

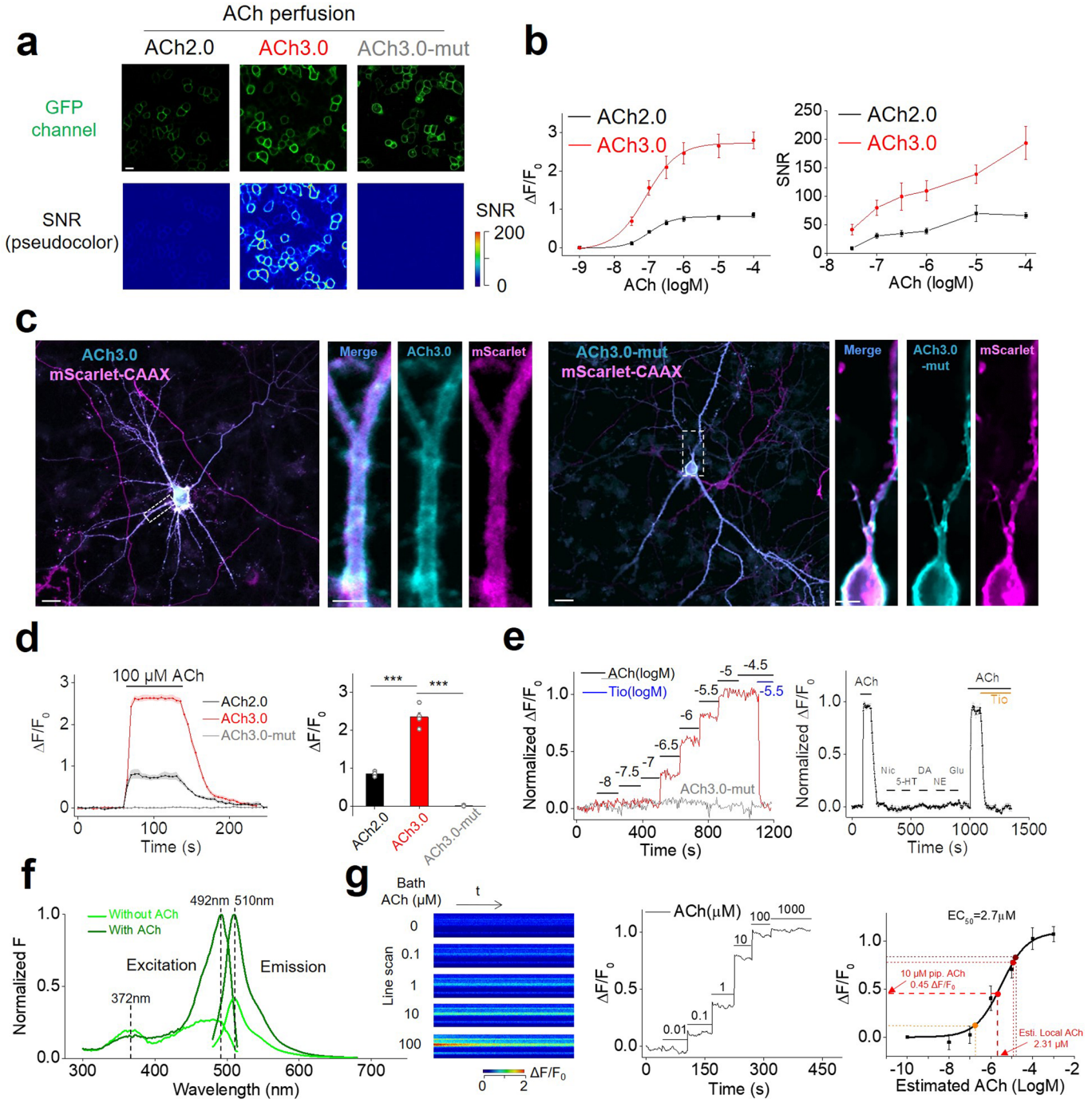

Extended Data Fig. 3 | See next page for caption.

Extended Data Fig. 3 | Characterization of ACh2.0 and ACh3.0. a, The fluorescence response of ACh2.0, ACh3.0, and ACh3.0-mut to 100 μM ACh in HEK293T cells. The fluorescence images are shown on top, and corresponding pseudocolor images representing the signal-to-noise ratio (SNR) are shown at the bottom. Similar results as the representative images were observed for more than 7 cells. Scale bars represent 10 μm. **b**, The peak fluorescence response ($\Delta F/F_0$, left) and SNR (right) of ACh2.0 (black) and ACh3.0 (red) are measured with the indicated concentrations of ACh; n = 8 and 7 cells for ACh2.0 and ACh3.0, respectively. **c**, Example fluorescence images of ACh3.0 (left) and ACh3.0-mut (right) expressed in cultured rat cortical neurons. Membrane-targeted mScarlet-CAAX is co-expressed and used to confirm expression at the plasma membrane. Similar results as the representative images were observed for more than 5 neurons. Scale bars represent 10 μm in the original image and 5 μm in the magnified images. **d**, Representative traces (left) and group summary (right) of the fluorescence response of ACh2.0, ACh3.0, and ACh3.0-mut expressed in cultured neurons; where indicated, 100 μM ACh is applied to the cells (n = 4, 5, and 7 neurons for ACh2.0, ACh3.0, and ACh3.0-mut, respectively), p=9.45E-5 between ACh2.0 and ACh3.0; p=6.42E-5 between ACh3.0 and ACh3.0-mut. **e**, Left, representative traces of the normalized fluorescence change in ACh3.0 (red) and ACh3.0-mut (gray) in response to application of the indicated concentrations of ACh. Note that the ACh-induced fluorescence response in ACh3.0 is blocked by the M_3R antagonist tiotropium (Tio, 3 μM). Right, representative trace of the normalized fluorescence change in ACh3.0 in response to indicated compounds. ACh: 100 μM; nicotine (Nic): 50 μM; 5-HT: 1 μM; norepinephrine (NE): 10 μM; dopamine (DA): 20 μM; glutamate (Glu): 10 μM; and Tio: 2 μM. Similar results as the representative images were observed for more than 5 neurons. **f**, The excitation and emission spectra of ACh3.0 sensor in the absence (light green) and presence of ACh (100 μM, dark green). **g**, Left, pseudocolor images showing the fluorescence response of ACh3.0 in confocal line scanning mode, with indicated concentrations of ACh applied by bath application. Middle, exemplar fluorescence response trace of ACh3.0 to different concentrations of ACh applied. Right, group data of the ACh3.0 dose-dependent fluorescence response in line scanning mode (from n = 4 coverslips), which is used to estimate the local ACh concentration reaching the cells during kinetics experiments. The steady-state fluorescence response of ACh3.0 to puffed ACh are shown and calibrated based on the curve, with the detail numbers of 10 μM pipette ACh list as an example (pipette short as pip.; Estimated short as Esti.) All data are shown as mean value ± SEM, with the error bars or shaded regions indicating SEM. Two-sides Student's t test performed in (d); ***p<0.001.

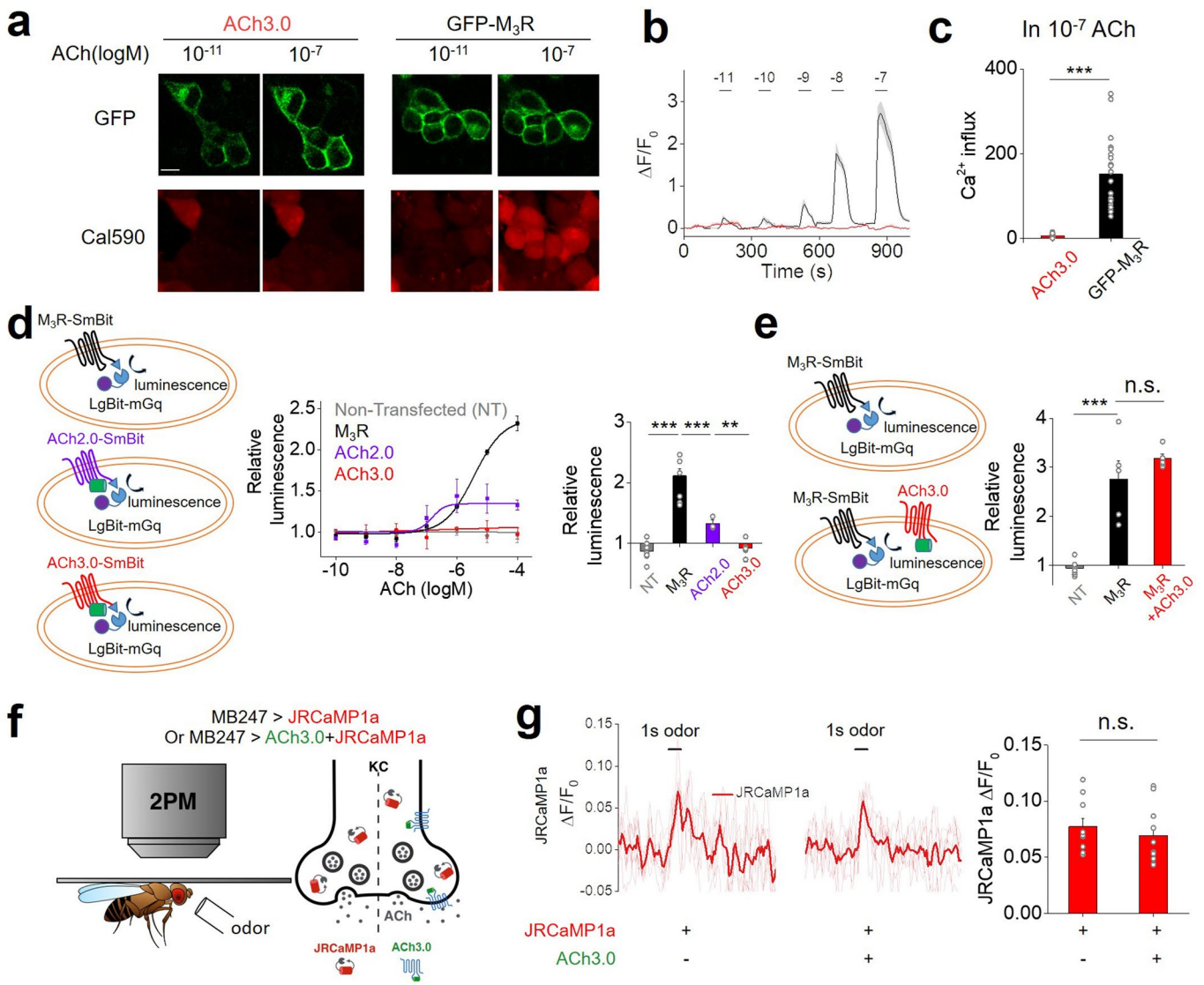

Extended Data Fig. 4 | The GRAB$_{ACh3.0}$ sensor produces negligible downstream signaling. a–c, HEK293T cells expressing either a GFP-tagged M_3R construct or ACh3.0 are loaded with the red Ca^{2+} dye Cal590 (a), and the change in Cal590 fluorescence is measured in response to various concentrations of ACh (b). The Ca^{2+} influx is calculated as the integration of Cal590 fluorescent signal ($\Delta F/F_0$) to ACh application. The group summary data for Ca^{2+} influx measured in response to 0.1 μM ACh are shown in panel c; n = 21 and 15 cells for GFP-M_3R and ACh3.0, respectively, p=1.06E-7. **d**, Left, cartoon illustrating the experimental design of the luciferase complementation assay, in which cells expressed M_3R-SmBit or ACh2.0/3.0-SmBit together with LgBit-mGq. Middle, the luminescence signal measured in non-transfected HEK293T cells (NT), cells expressing ACh2.0/ACh3.0-SmBit, or cells expressing M_3R-SmBit in response to application of the indicated concentrations of ACh, normalized to the signal measured in control buffer-treated cells (n = 6 wells for NT; n = 6 wells for M_3R; n = 3 wells for ACh2.0; n = 6 wells for ACh3.0, with >100 cells in each well). Right, group summary of the luminescence signal measured in response to 100 μM ACh (n = 6 wells for NT; n = 6 wells for M_3R; n = 3 wells for ACh2.0; n = 6 wells for ACh3.0, with >100 cells in each well; p=7.11E-7 between NT and M_3R; p=9.95E-7 between M_3R and ACh2.0; p=0.003 between ACh2.0 and ACh3.0). **e**, Similar to (d), except the luminescence signal is measured in HEK293T cells expressing M_3R-SmBit or cells expressing both M_3R-SmBit and ACh3.0. The group summary at the right shows the luminescence signal in response to 100 μM ACh; n = 5-8 wells per group, with each group averaging >100 cells, p=7.95E-5 between NT and M_3R; p=0.33 between M_3R and M_3R+ACh3.0. **f**, Schematic cartoon depicting two-photon imaging of transgenic flies in response to odorant stimulation. Ca^{2+} influx is measured by expressing jRCaMP1a either alone or together with ACh3.0 in the Kenyon cells (KC) of the mushroom body. **g**, Representative fluorescence traces (left) and group summary (right) of jRCaMP1a fluorescence measured in response to odorant application in flies expressing jRCaMP1a either alone or together with ACh3.0; n = 10 flies per group, p=0.49. All data are shown as mean value ± SEM, with the error bars or shaded regions indicating SEM. Scale bar represents 10 μm. Two-sides Student's t test performed in (c), (d), (e) and (g); ***p<0.001 and n.s., not significant.

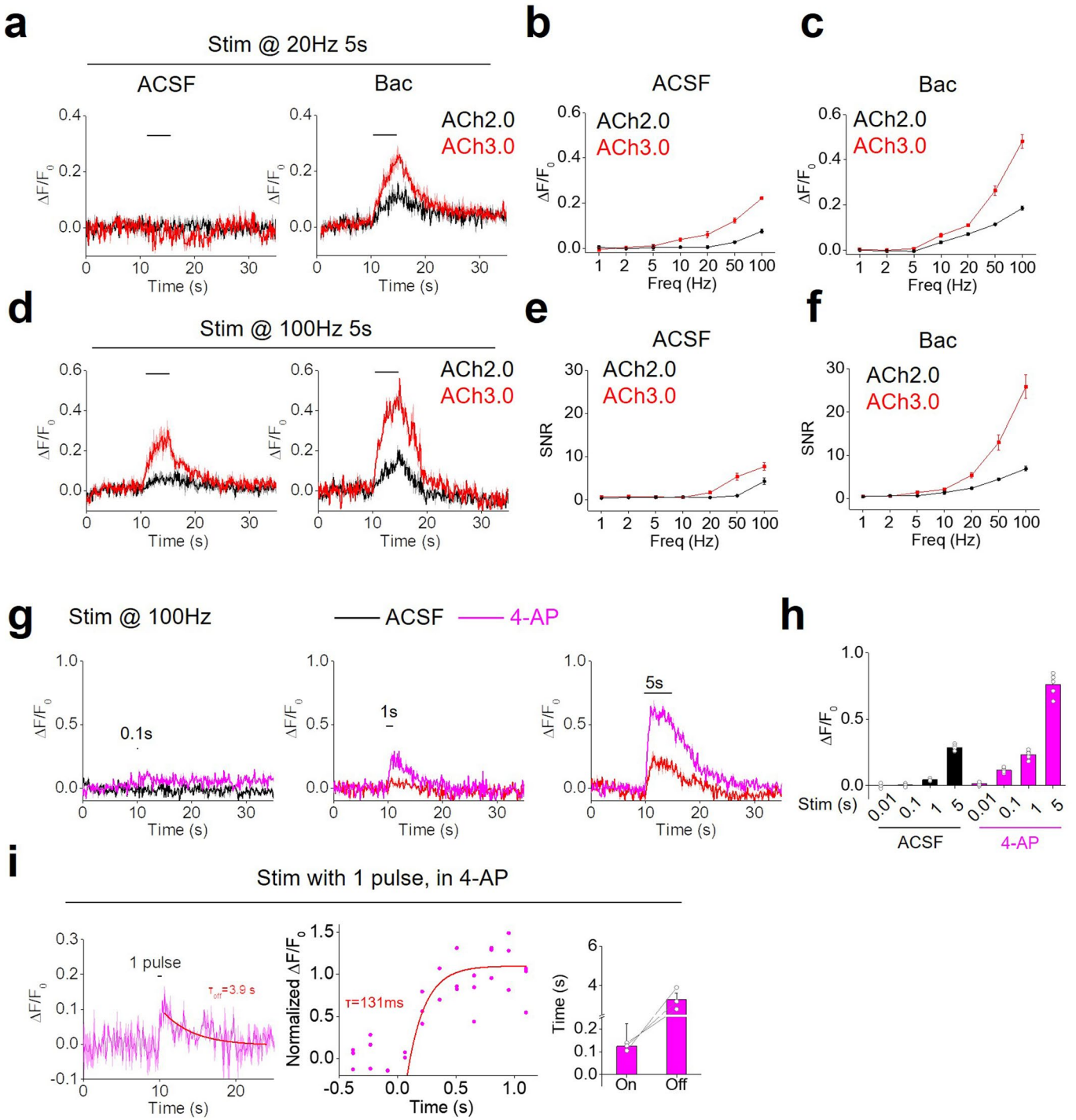

Extended Data Fig. 5 | Probing endogenous ACh release in mouse brain slices. a–f, Representative fluorescence traces (a, d) and group summary (b, c, e, f) of the fluorescence change ($\Delta F/F_0$ and SNR) in neurons expressing either ACh2.0 or ACh3.0 in response to electrical stimulation in MHb-IPN brain slices. The slices are bathed in either ACSF or 2 μM baclofen (Bac). N=5 slices from 3 mice for ACh2.0, and n = 10 slices from 7 mice for ACh3.0. **g**, **h**, The representative fluorescence traces (g) and group data (h) of ACh3.0-expressing neurons in response to 100-Hz electrical stimulation with different stimulation times in MHb-IPN brain slices. The response in either ACSF or 100 μM 4-AP is measured and summarized; n = 5 slices from 5 mice. **i**, The kinetics of fluorescence response of ACh3.0 to a single pulse (2 ms) of electrical stimulation in the presence of 100 μM 4-AP. The response in three independent experiments are normalized and plotted together in the middle. The group data of on and off response time constants are summarized on the right (n = 3 slices from 3 mice). All data are shown as mean value ± SEM, with the error bars or shaded regions indicating SEM.

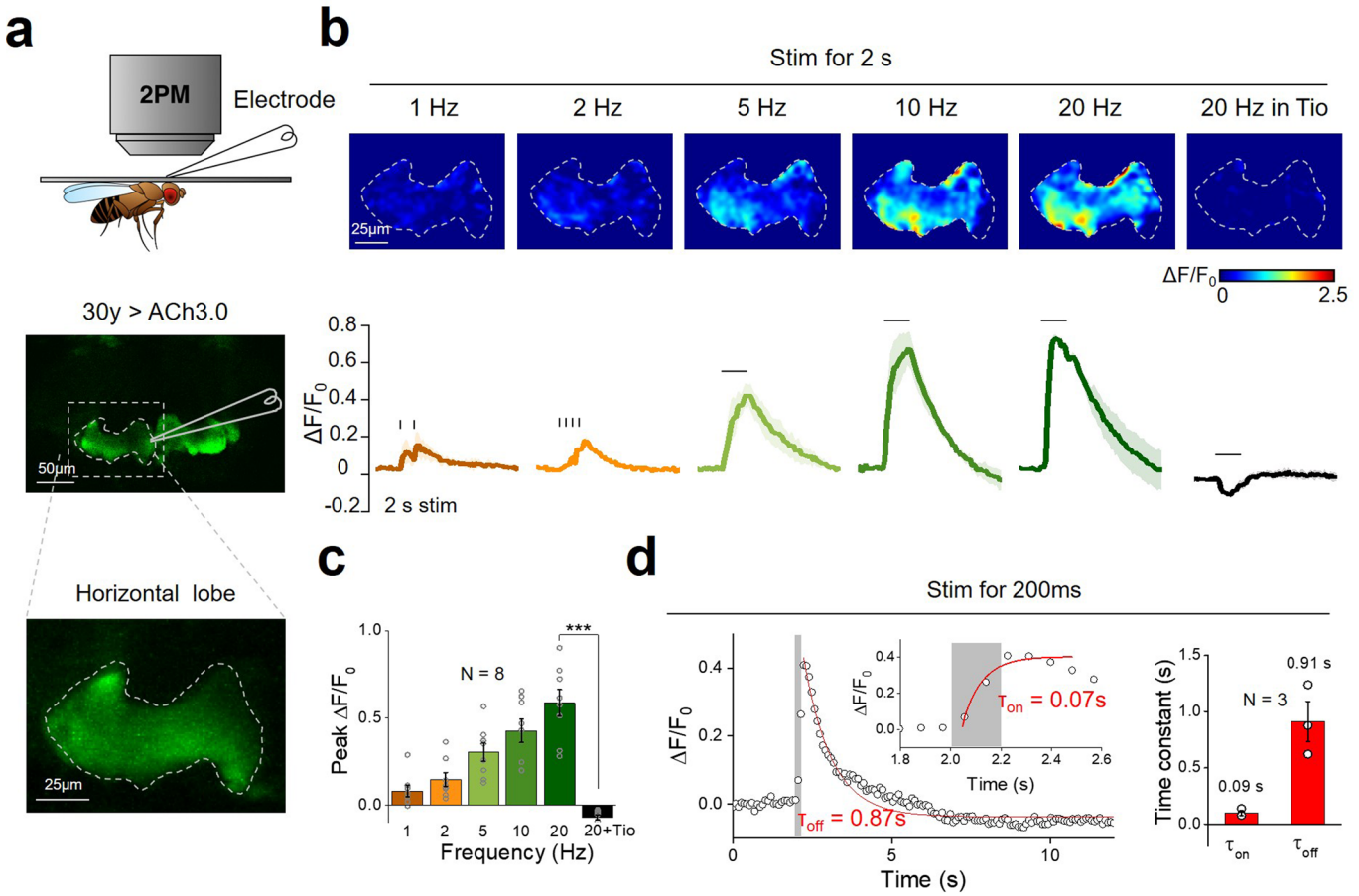

Extended Data Fig. 6 | Monitoring *in vivo* ACh release induced by electrical stimulation in *Drosophila*. a, Schematic illustration depicting the experiment in which a transgenic fly expressing ACh3.0 in the KC cells in the mushroom body is placed under a two-photon microscope, and a glass electrode is placed near the mushroom body and used to deliver electrical stimuli. The fly brain is bathed in AHLS containing 100 μM nicotinic acetylcholine receptor blocker mecamylamine (Meca). **b**, Pseudocolor images (top) and representative traces (bottom) of the fluorescence change in ACh3.0 in response to 2 s of electrical stimulation at the indicated frequencies. Where indicated, the M_3R antagonist tiotropium (Tio, 10 μM) is applied to the bath solution. Similar results as the representative images were observed for 8 flies. **c**, Group summary of the data shown in panel (b); n = 8 flies, p=0.0004. **d**, ACh3.0 fluorescence is measured before and after a 200-ms electrical stimulation, and the rise and decay phases are fitted with a single-exponential function; the time constants are indicated and summarized on the right; n = 3 flies. All data are shown as mean value ± SEM, with the error bars or shaded regions indicating SEM. Two-sides Student's t test performed in (c); ***p<0.001.

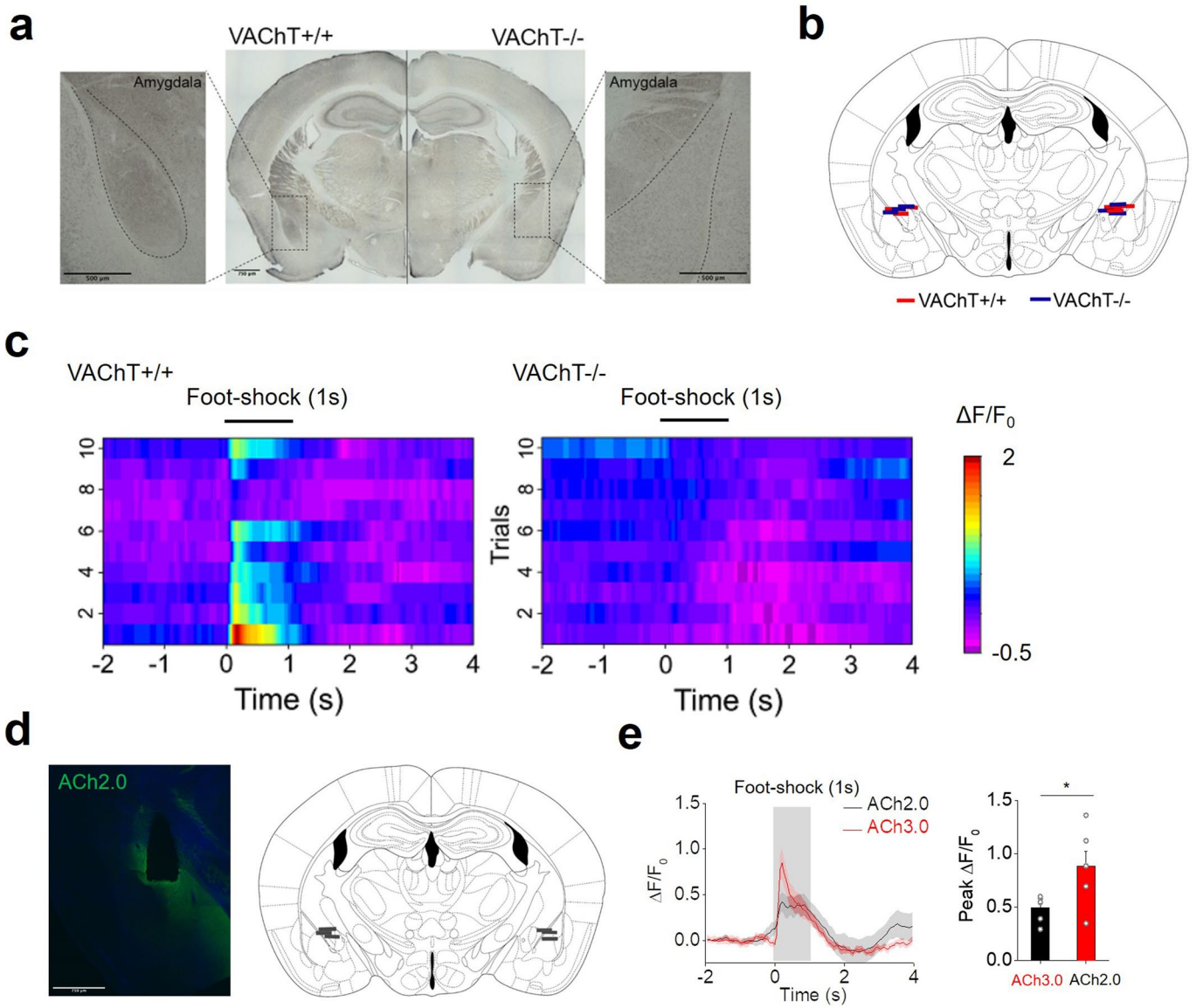

Extended Data Fig. 7 | Monitoring endogenous cholinergic signals in BLA of mice *in vivo*. a, VAChT immunohistochemistry is performed in coronal mouse sections obtained from a control ($VAChT^{+/+}$) mouse (left) and a $VAChT^{-/-}$ mouse (right). The insets show magnified views of cholinergic terminals in the basolateral amygdala (BLA). Similar results as the representative images were observed for 6 mice. Scale bars represent 500 μm. **b**, Diagram summarizing the location of the optic fiber terminals in the BLA of $VAChT^{+/+}$ (red) and $VAChT^{-/-}$ mice (blue); n = 6 mice per group. This image is modified from the brain map in Allen mouse brain atlas (Allen Mouse Brain Atlas (2004), Allen Institute for Brain Science). **c**, Pseudocolor image showing the change in ACh3.0 fluorescence measured in the BLA of $VAChT^{+/+}$ mice (left) and $VAChT^{-/-}$ mice (right) in response to a 1-s foot-shock; ten consecutive trials are shown. **d**, **e**, The comparison of ACh2.0 and ACh3.0 fluorescence response in BLA of mice to foot-shock stimuli. The fluorescence signal showing the expression of ACh2.0 and the fiber photometry recording sites are shown in (d). Fluorescence traces and group data of the 1 s foot-shock induced fluorescence response in ACh2.0 (black) and ACh3.0 (red) are shown in (e) (n = 6 mice each for ACh3.0 and ACh2.0, p=0.04). Scale bar: 750 μm. All data are shown as mean value ± SEM, with the error bars or shaded regions indicating SEM. Two-sides Student's t test performed in (e); *, p<0.05.

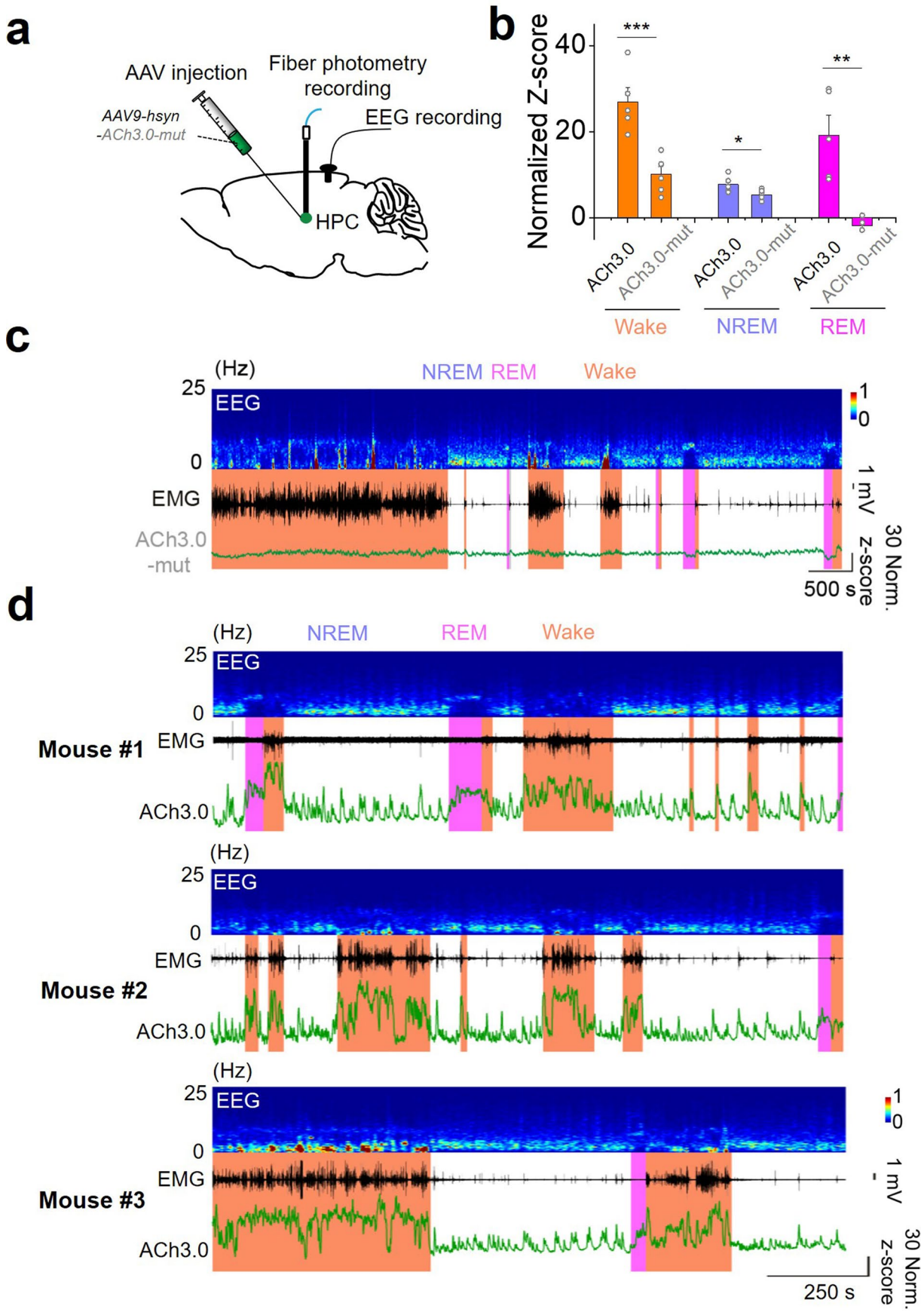

Extended Data Fig. 8 | See next page for caption.

Extended Data Fig. 8 | Recording of ACh signal during sleep-wake cycle. a, The schematic illustration and representative recording data of ACh3.0-mut sensor during the sleep-wake cycle in mice. **b**, The group data of the fluorescence response of ACh3.0 and ACh3.0-mut sensors in different sleep-wake status (n = 5 mice for ACh3.0 and n = 6 mice for ACh3.0-mut, p=0.0009 in wake; p=0.049 in NREM; p=0.008 in REM). **c**, The representative recording data of ACh3.0-mut sensor during the sleep-wake cycle in mice. Similar results as the representative images were observed for 6 mice. **d**, Multiple recording traces of the ACh3.0 sensor during the sleep-wake cycle (from 3 mice, additional to the representative one in Fig. 3g). All data are shown as mean value ± SEM, with the error bars or shaded regions indicating SEM. Two-sides Student's t test performed in (b); *, p<0.05; **, p<0.01; ***, p<0.001.

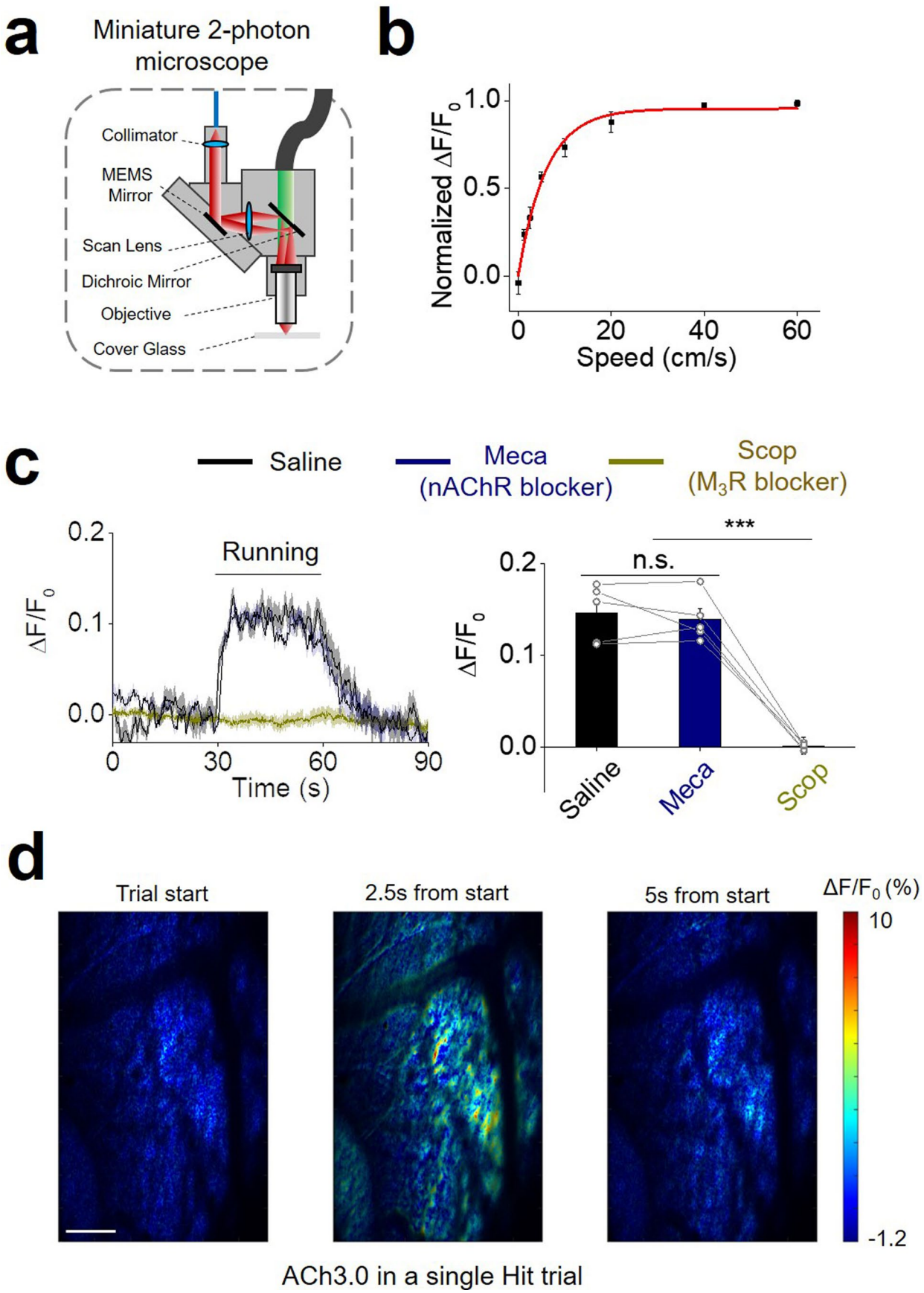

Extended Data Fig. 9 | See next page for caption.

Extended Data Fig. 9 | Imaging of ACh signal in the cortex. a, Cartoon illustration of the miniature two-photon microscope. **b**, Group data of ACh3.0 fluorescence in mice recorded while running on a treadmill at indicated speeds (n = 5 mice). **c**, Representative traces and group summary of ACh3.0 fluorescence measured in mice while performing the running task; where indicated, the mice receive an i.p. injection of saline (black), the nAChR blocker mecamylamine (Meca, 2 mg/kg body weight, blue), or the M_3R antagonist scopolamine (Scop, 20 mg/kg body weight, dark yellow); each trace is averaged from 10 trials; n = 5 mice per group, p=0.54 between Saline and Meca; p=0.0002 between Meca and Scop. **d**, Pseudocolor images showing the ACh3.0 fluorescence response in the S1 in the Hit trial of the whisker-guided object location discrimination task. The left, middle and right image showing the response during baseline, peak in the answer period and after response. Similar results as the representative images were observed for 3 mice. Scale bar: 100 μm. All data are shown as mean value ± SEM, with the error bars or shaded regions indicating SEM. Two-sides Student's t test performed in (c); *p<0.05, **p<0.01, ***p<0.001, and n.s., not significant.

nature research

Corresponding author(s): Miao Jing and Yulong Li

Last updated by author(s): Jun 28, 2020

Reporting Summary

Nature Research wishes to improve the reproducibility of the work that we publish. This form provides structure for consistency and transparency in reporting. For further information on Nature Research policies, see our Editorial Policies and the Editorial Policy Checklist.

Statistics

For all statistical analyses, confirm that the following items are present in the figure legend, table legend, main text, or Methods section.

n/a	Confirmed
☐	☒ The exact sample size (*n*) for each experimental group/condition, given as a discrete number and unit of measurement
☐	☒ A statement on whether measurements were taken from distinct samples or whether the same sample was measured repeatedly
☐	☒ The statistical test(s) used AND whether they are one- or two-sided *Only common tests should be described solely by name; describe more complex techniques in the Methods section.*
☐	☒ A description of all covariates tested
☐	☒ A description of any assumptions or corrections, such as tests of normality and adjustment for multiple comparisons
☐	☒ A full description of the statistical parameters including central tendency (e.g. means) or other basic estimates (e.g. regression coefficient) AND variation (e.g. standard deviation) or associated estimates of uncertainty (e.g. confidence intervals)
☐	☒ For null hypothesis testing, the test statistic (e.g. *F*, *t*, *r*) with confidence intervals, effect sizes, degrees of freedom and *P* value noted *Give P values as exact values whenever suitable.*
☒	☐ For Bayesian analysis, information on the choice of priors and Markov chain Monte Carlo settings
☐	☒ For hierarchical and complex designs, identification of the appropriate level for tests and full reporting of outcomes
☒	☐ Estimates of effect sizes (e.g. Cohen's *d*, Pearson's *r*), indicating how they were calculated

Our web collection on statistics for biologists contains articles on many of the points above.

Software and code

Policy information about availability of computer code

Data collection	Matlab 2013 (Mathwork) with custom written code and Synapse software were used for data collection.
Data analysis	The imaging data was processed by ImageJ and Matlab 2013, and plotted in Origin 9.1 (Originlab).

For manuscripts utilizing custom algorithms or software that are central to the research but not yet described in published literature, software must be made available to editors and reviewers. We strongly encourage code deposition in a community repository (e.g. GitHub). See the Nature Research guidelines for submitting code & software for further information.

Data

Policy information about availability of data

All manuscripts must include a data availability statement. This statement should provide the following information, where applicable:

- Accession codes, unique identifiers, or web links for publicly available datasets
- A list of figures that have associated raw data
- A description of any restrictions on data availability

The plasmid pAAV-hsyn-ACh3.0 and pAAV-hsyn-DIO-ACh3.0 have been deposited to addgene (#121922 and #121933) and are available. The custom-written MATLAB, Arduino, and TDT programs will be provided upon request.

Field-specific reporting

Please select the one below that is the best fit for your research. If you are not sure, read the appropriate sections before making your selection.

☒ Life sciences ☐ Behavioural & social sciences ☐ Ecological, evolutionary & environmental sciences

For a reference copy of the document with all sections, see nature.com/documents/nr-reporting-summary-flat.pdf

Life sciences study design

All studies must disclose on these points even when the disclosure is negative.

Sample size	No statistical methods were used to predetermine sample size. Sample sizes are indicated for each experiment and were chosen based on similar studies.
Data exclusions	No data was excluded from the analysis.
Replication	Each data in this manuscript is reliably reproducible. The replication number of each data is indicated in the legend of corresponding figures.
Randomization	Animals or cells were randomly assigned into experimental or control groups.
Blinding	No blinding was carried out for sensor development and characterization part, since the engineer process is to screen for well-performing candidates based on the subjective value, not by comparison. For slice and in vivo experiments, investigators were blinded to the group allocation during experiments.

Reporting for specific materials, systems and methods

We require information from authors about some types of materials, experimental systems and methods used in many studies. Here, indicate whether each material, system or method listed is relevant to your study. If you are not sure if a list item applies to your research, read the appropriate section before selecting a response.

Materials & experimental systems

n/a	Involved in the study
☐	☒ Antibodies
☐	☒ Eukaryotic cell lines
☒	☐ Palaeontology and archaeology
☐	☒ Animals and other organisms
☒	☐ Human research participants
☒	☐ Clinical data
☒	☐ Dual use research of concern

Methods

n/a	Involved in the study
☒	☐ ChIP-seq
☒	☐ Flow cytometry
☒	☐ MRI-based neuroimaging

Antibodies

Antibodies used	Primary antibody including (1) rabbit anti-VAChT antibody (Synaptic Systems, #139103; 1:250), (2)chicken anti-GFP (Abcam, #ab13970, 1:500) were used. Secondary antibody (1)Alexa 488 goat anti-chicken (Life Technologies, #A11039; 1:500) and (2) anti-rabbit biotynylated antibody (Vector Laboratories, #ba-9400; 1:200) were used.
Validation	The rabbit anti-VAChT antibody (Synaptic Systems, #139103) used in immunohistochemistry has been verified in Gras C, et al, Nature Neuroscience, 2008 and Frahm S, et al, eLife, 2015. The chicken anti-GFP(Abcam, #ab13970) used in immunofluorescence has been verified in Al-Moyed H, et al, EMBO Mol Med, 2019 and Handara G, et al, Dev Biol, 2019.

Eukaryotic cell lines

Policy information about cell lines

Cell line source(s)	HEK293T cell line bought from ATCC (catalog: CRL-3216) were used in this paper. The HTLA cell (HEK293 cells stably expressing a tTA-dependent luciferase reporter and a β-arrestin2-TEV fusion construct) were a gift from Bryan L. Roth in School of medicine at University of North Carolina.
Authentication	We have authenticated Hek293T and HTLA cell lines based on the morphology under microscope and the analysis of the growth curve.
Mycoplasma contamination	No mycoplasma contamination.

Commonly misidentified lines (See ICLAC register)	No commonly misidentified cell lines were used.

Animals and other organisms

Policy information about studies involving animals; ARRIVE guidelines recommended for reporting animal research

Laboratory animals	Male and female Sprague–Dawley rats (postnatal day 0, P0) were used to prepare cultured cortical neurons; P28-48 wild-type C57BL/6N mice were used to prepare the acute brain slices and two-photon in vivo imaging. C57BL/6J mice were used for fiber photometry recording. Mice lacking the vesicular acetylcholine transporter in the forebrain were generated by crossing VAChTflox/flox mice (Chat/Slc18a3tm1.2Vpra generated in a mixed C57BL/6J × 129/ SvEv background, backcrossed to C57BL/6J for 10 generations) with Nkx2.1-Cre mice (The Jackson Laboratory, stock no. JAX008661), yielding VAChT-/- offspring and control (VAChTflox/flox) littermates (referred to here as VAChT+/+). All mice were either family-housed or pair-housed in a temperature-controlled room (21.5 degree centigrade) with a 12-h/12-h light/dark cycle, with humidity controlled as 55%.
Wild animals	No wild animals are used in the study.
Field-collected samples	No field-collected samples are used in the study.
Ethics oversight	All procedures for animal surgery and experimentation were performed using protocols approved by the Animal Care & Use Committees at Peking University, the Chinese Academy of Sciences (CAS), Huazhong University of Science and Technology, and the University of Western Ontario (2016-104), and were performed in accordance with the guidelines established by US National Institutes of Health.

Note that full information on the approval of the study protocol must also be provided in the manuscript.